

## MIT Open Access Articles

*Efficient measurement of hydrodynamic coefficients for vibrating cylinders at supercritical Reynolds numbers*

The MIT Faculty has made this article openly available. **Please share** how this access benefits you. Your story matters.

**Citation:** Resvanis, Themistocles L. and Vandiver, J. Kim. 2022. "Efficient measurement of hydrodynamic coefficients for vibrating cylinders at supercritical Reynolds numbers." Journal of Fluids and Structures, 108.

**As Published:** 10.1016/j.jfluidstructs.2021.103427

**Publisher:** Elsevier BV

**Persistent URL:** <https://hdl.handle.net/1721.1/154920>

**Version:** Final published version: final published article, as it appeared in a journal, conference proceedings, or other formally published context

**Terms of use:** Creative Commons Attribution-NonCommercial-NoDerivs License





# Efficient measurement of hydrodynamic coefficients for vibrating cylinders at supercritical Reynolds numbers

Themistocles L. Resvanis<sup>\*</sup>, J. Kim Vandiver

Department of Mechanical Engineering, Massachusetts Institute of Technology, Cambridge, MA, USA

## ARTICLE INFO

### Article history:

Received 14 January 2020

Received in revised form 5 October 2021

Accepted 26 October 2021

Available online 2 December 2021

### Keywords:

Vortex-induced vibration

VIV

Hydrodynamic coefficients

Supercritical Reynolds number

Ramp-tests

Time-varying flows

High Reynolds number

## ABSTRACT

Free-response Vortex-Induced Vibration (VIV) tests were conducted on a 6.233 m long cylinder with a diameter of 0.325 m. The cylinder was allowed to vibrate in the cross-flow direction and towed at Reynolds numbers varying from 200,000 to 700,000. Rather than conducting hundreds of individual tests at discrete values of reduced velocity, the free-response was measured while continuously varying the towing speed in a manner that ensures quasi-steady response. These 'ramp-tests' not only yielded response data corresponding to continuously varying reduced velocity, but also yielded observations of the hysteresis effects associated with increasing or decreasing flow speed. The results from the carefully conducted 'ramp-tests' are compared with steady towing speed results to confirm their validity. The cylinder's free-response was controlled by systematically varying the external electro-mechanical damping. Lift and added mass coefficients at supercritical Reynolds numbers were extracted using the known relationships between cylinder response and hydrodynamic loading. Contour plots of lift and added mass coefficients are presented as a function of dimensionless response amplitude and reduced velocity. Stationary cylinder drag coefficients were also efficiently acquired using the ramp testing technique. These results are presented and compared with the VIV amplified drag coefficients.

© 2021 The Author(s). Published by Elsevier Ltd. This is an open access article under the CC BY-NC-ND license (<http://creativecommons.org/licenses/by-nc-nd/4.0/>).

## 1. Introduction

The principal goals of this project were to advance model testing techniques for very high Reynolds number Vortex-Induced Vibration (VIV) and to acquire lift coefficient data at trans-critical and supercritical Reynolds numbers (i.e. order  $10^5$  to  $10^6$ ), which are particularly relevant to the design of long slender structures exposed to ocean currents such as, drilling and production risers used by the offshore Oil & Gas industry or for the design of the large diameter cold-water intake pipes and risers necessary for Ocean Thermal Energy Conversion plants.

When vortices are shed behind the trailing edge of a fluid immersed body, the structure is subjected to strong periodic forces. If the frequency of shed vortices coincides with one of the structure's natural frequencies, large response amplitudes can result that can lead to considerable damage accumulation in a process known as Vortex-Induced Vibrations (VIV). Long-slender structures such as risers, umbilicals and cables are particularly prone to VIV and the accumulated fatigue damage is often the most critical parameter driving the design process. Despite the significant improvements that have been made over the past few decades to commercially available computational fluid dynamics (CFD) packages, the iterative design process and the necessity to evaluate hundreds or even thousands of different current profiles still make the use of

<sup>\*</sup> Corresponding author.

E-mail address: [resvanis@mit.edu](mailto:resvanis@mit.edu) (T.L. Resvanis).

CFD prohibitive for riser design. To date, semi-empirical computer programs such as SHEAR7, VIVA and VIVANA remain the most popular options for predicting VIV on offshore risers and the associated fatigue damage. These semi-empirical tools employ a strip-theory approach which requires hydrodynamic data that is most often obtained from tests on rigid cylinders.

Recent model testing of elastically mounted rigid cylinders (Klamo et al., 2005; Govardhan and Williamson, 2006; Blevins and Coughran, 2009; Raghavan and Bernitsas, 2010) and of flexible cylinders (Swithenbank et al., 2008; Resvanis et al., 2012) undergoing VIV has shown that the resulting response amplitude is strongly influenced by the Reynolds number in the subcritical Reynolds range. One of the primary motivations of studying VIV at higher Reynolds numbers is to discover the Reynolds number dependence of hydrodynamic coefficients in the Reynolds number range between  $10^5$  to  $10^6$ .

High Reynolds number model testing is very expensive and many technical obstacles need to be overcome to be able to acquire useful high Reynolds number data. Because the mass-ratio is extremely important to the VIV response of cylinders it is important that high Reynolds tests for ocean engineering applications be performed in water rather than air, which in turn requires test frames that can withstand large dynamic loads. This paper describes two recent contributions to the field of VIV model testing. The first shows how *free-response* VIV model testing can be used to obtain the hydrodynamic coefficients of interest at full scale Reynolds numbers. The second contribution describes how the towing speed can be continuously varied in a controlled manner and thus cover a large range of flow conditions in a single run down the towing tank. This greatly reduces the number of runs necessary to obtain the hydrodynamic coefficients of interest.

The model tests described in this paper were intended as proof-of-concept tests and are the result of a rare opportunity to do these tests at low cost, because of the alignment in time and objectives of two related projects. The first round of testing was conducted in just two and a half days in March 2015 and was later followed by an additional day of testing in December of 2015, which provided the opportunity to improve the test matrix based on lessons learned in the first rounds of tests. Between the two visits to the testing facility, sufficient data was gathered to demonstrate the validity of the new methods. The results include valuable VIV lift coefficient data at supercritical Reynolds numbers and show the way forward to significantly improve the efficiency of future VIV model tests.

It is outside the scope of this paper to include a full literature review of VIV. The topic has been studied extensively over the past few decades and the introductory material is covered well in the books by Blevins (1990), Paidoussis (2003) and Sumer and Fredsoe (2006). The interested reader is referred to the excellent review papers by Williamson and Govardhan (2004) and Sarpkaya (2004) amongst the many others available. The results from the tests described in this investigation will be compared with the most relevant and publicly available experimental data in the discussion section.

There are two approaches to acquiring VIV lift coefficient measurements from towing tank tests or flumes, namely *forced-vibration* model tests and *free-response* model tests. In *forced-vibration* model testing the cylinder or riser model is towed at predetermined speeds while an external control mechanism forces the cylinder to vibrate at a specific frequency and amplitude. Measurement of the hydrodynamic loads allows the extraction of hydrodynamic coefficients for each test combination of prescribed frequency, amplitude, and towing velocity. *Forced-vibration* tests have long been the accepted practice for the determination of lift coefficients. The general theory and practice are nicely covered in the work of Gopalkrishnan (1993). The original lift coefficient databases used by the semi-empirical VIV prediction programs SHEAR7, VIVA and VIVANA were all derived from such forced VIV measurements. The sheer size of the test matrices resulting from the combination of forced frequencies, vibration amplitudes, and different towing speeds has usually limited such testing to small laboratory testing facilities that are inexpensive to operate but are unable to reach high Reynolds numbers. Notable exceptions are the 2-DOF *forced-vibration* tests performed by Dahl et al. (2006) that reached Reynolds numbers up to  $6 \times 10^4$ , the industry sponsored tests by DeepStar (2003) at  $2 \times 10^5 < Re < 10^6$  and more recently by Yin et al. (2018) who conducted cross-flow forced motion tests at Reynolds numbers up to  $4 \times 10^5$ .

In *free-response* (or *free-vibration* or *self-excited*) VIV model testing the cylinder or riser model is towed through the towing tank and the spring-mounted cylinder is left entirely free to respond to the external fluid forces resulting from the vortex shedding. *Free-response* VIV tests have been the subject of countless investigations and more recently these investigations have additionally included damping as a control variable with the intention of computing force coefficients. Noteworthy mentions are the work by Blevins and Coughran (2009) and Blevins (2009) which resulted in very detailed lift and added mass coefficient in the subcritical regime. The first reported attempt to do this at high Reynolds numbers was in 2003, when ExxonMobil used the *free-vibration* method to conduct cutting-edge, very high Reynolds number, VIV tests at the David Taylor Model Basin in Carderock, Maryland. A total of 1760 runs were made and the tests were described by Ding et al. (2004). They presented a sample of the lift coefficient data in the published paper but did not publish the corresponding Reynolds numbers. They also did not explain the theory of how one extracts the lift coefficient data from measurements of *free-vibration* response. Vandiver (2012) describes the full theory of lift coefficient determination from *free-response* VIV measurements, including accounting for the effects of Reynolds number. He showed that by carefully controlling damping in the model test, the entire range of response amplitude and lift coefficient may be explored. This is the primary method used to compute lift coefficients in the experiments described in this paper.

In 2015, when the tests described in this paper were conducted, there were only two experimental facilities in the world available which had towing carriages able to withstand the large dynamic loads associated with high Reynolds number VIV testing. The one used to conduct the tests described in this report, is the National Research Council's towing tank in St. Johns, Newfoundland, Canada. This facility had been used previously by Oceanic Consulting Corp. in St. Johns, to

conduct a variety of tests for the offshore oil and gas industry. Although the Oceanic VIV test rig has been used extensively in the past to conduct *free-response* VIV tests, it has not been used in the manner described in this paper where damping is varied systematically with the sole intention of obtaining lift coefficient data from *free-response* VIV tests. Instead, the damping actuator (or damping compensation servo-motor) on Oceanic's VIV testing rig has traditionally been used to compensate or nullify the non-negligible energy lost due to the mechanical damping present in the experimental setup that results from the many linkages and mechanical connections. In other words, the *free-response* VIV data that had been previously collected was typically at near-zero damping conditions.

At near-zero damping, the corresponding lift coefficients are very small or nearly zero and the observed response amplitudes are at their maxima for each reduced velocity tested. Even though such tests reveal the maximum possible response amplitude and represent the most detrimental scenario they are not particularly relevant to the design of risers in real sheared ocean currents for several reasons. The VIV of a riser in a sheared or exponentially decaying current profile involves substantial lift coefficients in the excitation regions and significant hydrodynamic damping coming from the remote region far away from the excitation region. The industry needs model testing methods that yield accurate hydrodynamic coefficients appropriate for the intended, as-built, operating conditions. Advancing such model test methods was one of the principal goals of this project. The model tests described in this report were conducted at higher damping values and therefore higher lift coefficients which are more representative of the conditions that offshore marine risers are exposed to.

This paper presents results for the response of cylinders in slowly and carefully controlled time-varying flows. Time-varying flows and their effects on VIV are particularly relevant to the ocean and offshore engineering community, because ocean currents vary slowly with time. With the exception of the thorough investigations of fixed and free cylindrical sections in oscillatory flows which are nicely summarized in [Sarpkaya \(2004\)](#) and [Sumer and Fredsoe \(2006\)](#), the topic of more generally time-varying current excitation has been left almost entirely unexplored. In this investigation the main emphasis of exploring the response in time-varying flows was to prove that a few tests in slowly varying flow conditions can produce data equivalent to hundreds of individual steady speeds tests, thus drastically reducing the necessary tank time and testing costs.

The main focus of this paper is to:

- Show the use of variable speed towing tests and to compare the *free-response* results with the results from the steady towing speed tests in order to demonstrate that they are a suitable alternative to existing testing techniques.

- Demonstrate the computation of hydrodynamic force coefficients using the governing equations and the *free-response* data collected at two different supercritical Reynolds numbers.

- Review the sensitivity or existence of Reynolds number effects in the supercritical Reynolds number region through the results collected in this investigation and discuss any suitable and relevant data that currently exists in the literature.

- Demonstrate that when *free-response* tests are conducted with a suitably large variation in the system damping, the computed hydrodynamics coefficients can then be used to cover entire domain of response amplitude and reduced velocity where self-excited VIV are possible.

The material in this paper is arranged and presented in the following manner which we feel is best suited to accomplishing our goals:

- Section 2.1 contains the derivations and equations that are used to compute the hydrodynamic coefficients from the VIV response data that are measured during *free-response* VIV tests.

- Section 2.2 presents a summary of the variable speed testing technique and the dimensionless parameter that assures quasi-steady response.

- Section 3 describes the experimental apparatus and the testing facility used for these tests.

- Section 4.1 presents the results from the variable speed towing tests (*i.e.* ramp tests) which are compared with the steady speed tests as a reference. This section is used to demonstrate that the results from the ramp tests can be suitable alternatives to the many individual steady speed tests that are necessary to fully characterize the VIV response amplitude's dependence on the reduced velocity.

- Section 4.2 presents the VIV response amplitudes for various amounts of damping and demonstrates how the response information can be used to compute the lift coefficients at two different Reynolds numbers investigated in the first round of testing in March 2015.

- Section 4.3 shows the results from the follow-up tests in December 2015 and presents the complete added mass and lift coefficient surfaces that were computed. These results are intentionally presented on their own to demonstrate the repeatability of the measurements conducted in the first round of tests.

- Section 4.4 compares the experimentally determined lift and added mass coefficients with the high Reynolds number data that is available in the literature.

- Section 5 closes the main portion of the paper with our conclusions and recommendations for future work and improvements to the testing techniques presented.

- Appendix A presents the stationary cylinder drag coefficient and compares this with the drag coefficients recorded while the cylinder was undergoing VIV to demonstrate the well-known effect of VIV amplified drag. The fixed cylinder drag coefficients are included to verify that the test cylinder was tested in the supercritical Reynolds regime.

- Appendix B demonstrates the effects of plotting the cylinder's response data and the computed hydrodynamic coefficients as a function of the true reduced velocity instead of the nominal reduced velocity which is employed in the main body of the manuscript.

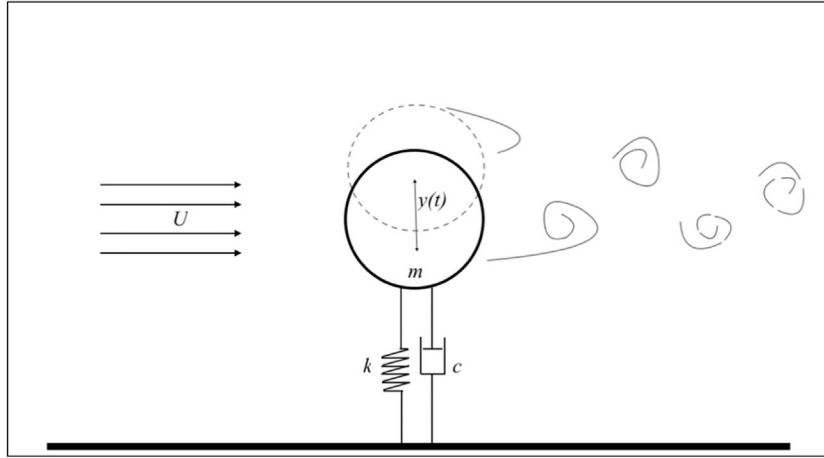


Fig. 1. Spring mounted cylinder responding to an external fluid flow.

## 2. Theoretical background

### 2.1. Extracting hydrodynamic coefficients from free-response VIV tests

The tests described in this report make use of a large spring-mounted cylinder, operating as a simple single-degree-of-freedom oscillator restricted to vibrate purely in the cross-flow direction. The oscillator mass,  $m$ , is a rigid cylinder, supported by springs of total stiffness,  $k$ , and a linear dashpot with damping constant,  $c$ . Fig. 1 depicts a simplified version of such an oscillator.

The VIV response of spring-mounted rigid cylinders has been the topic of hundreds of papers over the past sixty years. It has only been in the last ten to fifteen years that some real clarity has been achieved in the understanding of the complex relationship between the VIV response amplitude,  $A$ , Reynolds number,  $Re$ , lift coefficient,  $C_L$ , mass ratio,  $m^*$ , total damping coefficient,  $c$ , flow speed,  $U$  and the dynamic properties of the structure. In particular, the work of Klammo et al. (2005) and Govardhan and Williamson (2006) showed that the effect of Reynolds number on VIV response was separable from that of damping in the subcritical Reynolds range. Vandiver (2012) then cleared up some long-standing misconceptions about damping and proposed a new dimensionless damping parameter,  $c^* = \frac{c\omega}{\frac{1}{2}\rho U^2 L}$ .

The equation of motion describing the cross-flow motion  $y(t)$  of a cylinder with length  $L$ , diameter  $D$  that is being excited by a fluid of density  $\rho$  moving with velocity  $U$  can be modeled according to Eq. (1). The fluid exciting force is acting at a frequency  $\omega$  and lags the cylinder motion by an amount  $\varphi$  and is modeled in the usual manner via an excitation coefficient  $C_y$ :

$$m\ddot{y} + c\dot{y} + ky = \frac{1}{2}C_y\rho U^2 DL \sin(\omega t + \varphi) \quad (1)$$

The above equation leads to two distinct equations after substituting the particular solution for the cylinder displacement  $y(t) = A \sin(\omega t)$  and making use of the trigonometric identities

$$(k - m\omega^2)A = \frac{1}{2}C_y\rho U^2 DL \cos(\varphi) \quad (2)$$

$$c\omega A = \frac{1}{2}C_y\rho U^2 DL \sin(\varphi) \quad (3)$$

The first equation describes the dynamic equilibrium between stiffness and inertia forces and the portion of the fluid excitation that is in phase with the cylinder acceleration and is similar to the concept of effective stiffness discussed in Leonard and Roshko (2001). The second equation describes the dynamic equilibrium between the damping forces (i.e. dissipative forces) and the fluid excitation that is in phase with the cylinder velocity. These two equations can be further rearranged in the following form:

$$C_M \equiv C_y \cos(\varphi) = \frac{(k - m\omega^2)A}{\frac{1}{2}\rho U^2 L \frac{A}{D}} \equiv k_{eff}^* A^* \quad (4)$$

$$C_L \equiv C_y \sin(\varphi) = \frac{c\omega A}{\frac{1}{2}\rho U^2 L \frac{A}{D}} \equiv c^* A^* \quad (5)$$

These two simple expressions therefore provide a means of determining the added mass and lift coefficients from *free-response* VIV tests. All that is necessary is that one knows the damping, stiffness and mass of the system and that there is a means of recording the response amplitude and response frequency of the system at a given flow speed. For simplicity the analysis presented above assumed that the response was harmonic but it can easily be extended to any periodic signal using Fourier series. If Fourier series are used for more complex signals, care must be taken to properly attribute each response amplitude component to its corresponding force coefficient component.

The *free-response* VIV tests presented in this paper were conducted with two different spring constants and at several different levels of damping, characterized by the dimensionless damping parameter,  $c^*$ . Each set of springs will result in the self-excited vibrations occurring over a different range of towing velocities and hence Reynolds numbers. The product of  $c^*$  and the measured dimensionless response amplitude  $A^* = A/D$  yields the lift coefficient since  $C_L = A^* c^*$ . This formula is valid over the entire wake synchronization range of reduced velocity and the only assumption made is that the cylinder is vibrating at the same frequency as the forcing from the shed vortices modeled using the right-hand side of Eq. (1).

*Free-response* VIV is rarely observed to consist of constant amplitude sinusoidal behavior and some amplitude modulation is a common occurrence even if the environmental conditions are steady. A common statistical way of managing this is to compute the RMS of the cylinder's time-varying response. For sinusoidal or narrow-banded time-histories the vibration amplitude may be estimated as  $A^* = \frac{A}{D} = \frac{\sqrt{2} Y_{RMS}(t)}{D}$ . This approach is taken in this investigation and is further supplemented by computing all statistical quantities using a moving window of short duration that passes through the entire time-section as shown in Eq. (7). This is the response amplitude that is reported in all figures in this manuscript. The effects of any higher harmonics on the displacement time-series and hence on the  $A^*$  reported are negligible for the data collected in this particular investigation. If these contributions had been significant, then one would have had to separate the response signals into its fundamental component and the associated higher harmonics and proceed to compute the added mass and lift coefficients for each of the separate signal components.

## 2.2. Variable speed towing tests or 'ramp tests'

VIV model testing in support of industrial applications has been conducted in essentially the same way for the past sixty years. Data, characterizing the VIV response of a cylinder, has been traditionally acquired one flow velocity at a time. At most 4–5 tests per hour are possible in a large commercial towing tank because a large amount of time is spent waiting for the turbulence to settle down before commencing the next towing run. For each set of springs used in the test, it is good practice to test at 15 to 20 specific velocities that encompass the range of significant VIV response. However, it is often the case that in the interest of conserving tank time and limiting testing costs, only 5 or 6 different reduced velocities are selected for testing which makes it easy to miss the specific towing speed, which results in the maximum response.

This paper presents a new way of performing model tests using slowly varying towing velocities to reduce the number of required runs. This more efficient model testing technique was first described in Resvanis (2014) and in abridged form in Resvanis et al. (2015). That work showed that in two or three towing runs, it is often possible to acquire the necessary VIV response data that would require twenty constant speed tests, using conventional techniques for flexible cylinders undergoing VIV. The ramp technique smoothly provides data at all velocities, leaving no gaps, where unusual phenomena might be missed in a conventional test.

The testing procedure calls for slowly varying the towing speed during each run. The basic premise of the ramp test is to change the towing speed slowly, so that the VIV response can closely follow the slowly and progressively changing hydrodynamic forces in a quasi-steady manner. A dimensionless parameter,  $\gamma$ , was introduced in Resvanis (2014), which quantifies the rate of change in flow velocity,  $U$ , in a context relevant to VIV. This dimensionless parameter,  $\gamma$ , is defined in Eq. (6) and is a measure of the change in flow speed occurring in a representative time-scale. For *free-response* VIV tests the most suitable candidates for the time-scale are the cylinder's natural period or the actual period of vibration. The still water natural period,  $T_n$ , was used when planning the experiments described in this paper.

$$\gamma = \frac{dU/dt T_n}{U} \quad (6)$$

For rigid cylinders with a single natural frequency the ramp profile should be designed or chosen in a manner that attempts to keep the  $\gamma$  value nearly constant. The amount of control that one has over the ramp profile invariably depends on the type and flexibility of the towing carriage's speed controller (or the flume controller) at the testing facility. The changing carriage speed (or equivalently the flume current) can be determined by solving the simple differential equation shown in Eq. (6) in conjunction with the desired starting and ending speeds which will yield the integration constant. The carriage speed as a function of time was programmed into the carriage controller so as to keep  $\gamma$  within a value of 0.01 to 0.02. A  $\gamma$  value of 0.02 means that the towing speed changes by only 2% per period of vibration. These values were chosen because they have been previously found to yield satisfactory results for cylinders with mass ratio values between 1 and 2 (Resvanis, 2014). Fig. 2 shows the towing speed and response amplitude for one of the ramp tests conducted. The  $\gamma$  values are shown on the right-hand vertical axis. In this test, the towing carriage's acceleration was continuously increased in a manner that kept  $\gamma$  slightly under 0.02. The figure also shows  $\gamma$  values when computed based on the actual vibration



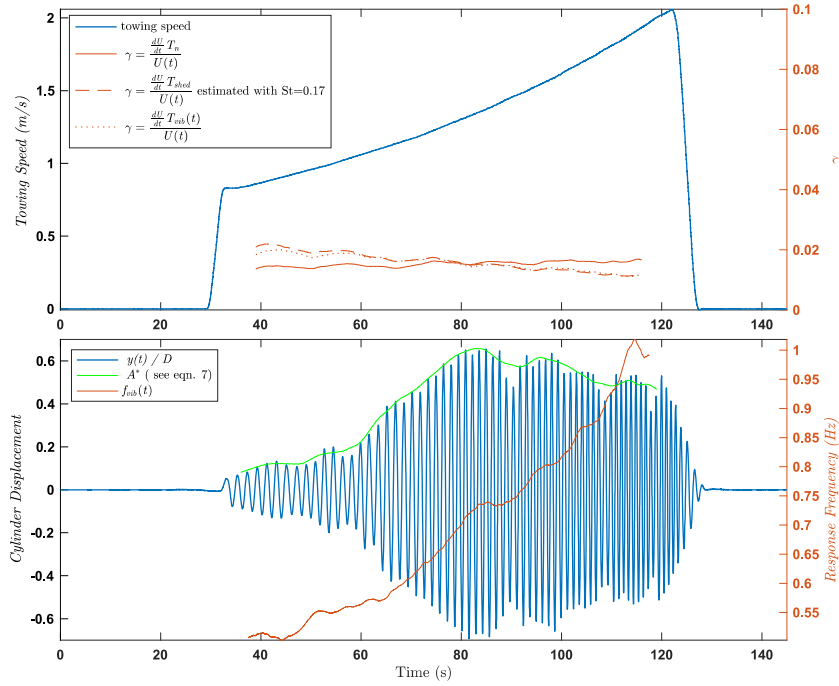


**Fig. 2.** Ramp test and recorded cylinder response for soft springs ( $f_n \sim 0.69$  Hz) and  $\zeta = 0.16$ . (For interpretation of the references to color in this figure legend, the reader is referred to the web version of this article.)

period,  $T_{vib}$ , as well as the value that would result if one had to estimate the vortex shedding period,  $T_{shed}$ , using a Strouhal number of 0.17.

The relationship between the maximum permissible  $\gamma$  that will result in quasi-steady response and the cylinder's mass-ratio and amount of damping present has not yet been fully investigated. It is known that a simple linear, one degree of freedom oscillator, excited by a sinusoidal force will approach steady state in fewer cycles as the damping ratio is increased. Similarly, low mass-ratio cylinders will react faster to changing hydrodynamics forces because the fluid added mass makes up a significant portion of the total inertia. In later sections of this manuscript the VIV response quantities obtained from ramp tests are compared to those from conventional constant speed tests. The comparisons reveal that ramp tests can yield reliable results if the towing speed is varied slowly.

### 2.3. Analysis of non-stationary time-series & inherent response variability

One objective of this work is intended to show that a few carefully planned variable speed tests can provide equivalent information to the *free-response* data traditionally obtained through a large number of constant speed tests. Since the external flow conditions are continuously changing, the entire data record must be treated as a non-stationary time-series. The cylinder response amplitude will approximately trace out the familiar response amplitude versus reduced velocity curve as the towing speed changes with time. All statistical quantities (RMS, mean *etc.*) are computed from within a moving window that is 'swept' through the entire time-series. Such statistical quantities are often referred to as moving or running quantities. The window length used in these experiments corresponded to 5 natural periods.

When the same approach is used to analyze data from the constant speed tests the analysis results can be used to assess the inherent variability in the response quantities (response amplitude, response frequency, drag and lift forces *etc.*) that exists even when the towing speed is held constant (Resvanis and Vandiver, 2017). The 'moving-window' that passes through the entire data record, essentially splits the data record into many smaller ones, each being  $\sim 5$  natural periods long. The statistical quantities of interest are calculated for each short time-record. By comparing the largest and smallest values of the moving statistical quantities acquired in the constant speed tests, one can get a measure of the inherent variability that exists in VIV response data. Furthermore, when such an approach is used, the analysis results do not depend on the analyst's subjective choice of which portion of the time-series to analyze. Instead, the entire available time-series is analyzed with the moving window operator and all computed quantities are reported.

Fig. 3 is an example of VIV response showing very little variability in the measured response amplitude. By comparison, Fig. 4 shows the cylinder response at a slightly higher reduced velocity. There is substantial variability even though lock-in conditions still exist and the towing speed is being held constant. The mechanisms leading to this response amplitude variability at the very high Reynolds numbers are not known or well understood. It is interesting to note that

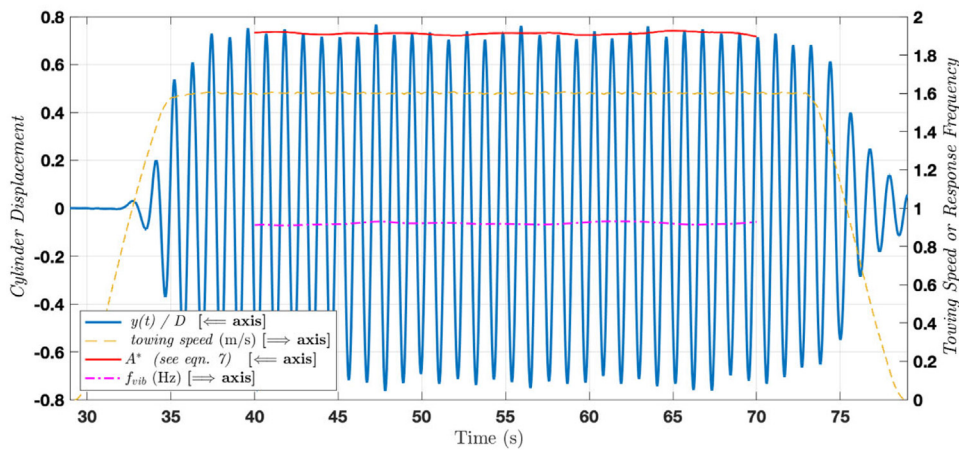


**Fig. 3.** A typical time-series from a conventional test with little variability in the response amplitude, test with stiff springs ( $f_n \sim 0.90$  Hz) &  $\zeta \sim 0.09$  at  $U \sim 1.6$  m/s ( $Re \sim 4.7 \times 10^5$ ) which corresponds to  $V_{Rn} \sim 5.5$ . (For interpretation of the references to color in this figure legend, the reader is referred to the web version of this article.)

the large variability in the response amplitude is not always associated with large variability in the response frequency. The response amplitude measurements in this investigation never showed strong beating behavior or distinct bistable state behavior or indications of strong chaotic behavior. The inherent response variability is limited to small amounts of amplitude modulation and even smaller amounts of frequency modulation as shown in Fig. 4. Because the emphasis of this manuscript is placed on the new physical model testing techniques that were employed, it is by intention that more elaborate non-stationary signal analysis techniques like wavelets *etc.* are not used. Another common technique is to report the 1/3rd or 1/10th largest response amplitudes, but this tends to mask the inherent variability. The computed RMS amplitude from a short duration moving window was sufficient to capture the inherent variability that existed in these tests. The principal comparison is between the cylinder's response in ramp tests and constant speed tests. At the same reduced velocity both testing methods exhibit variable response, which may be quantified by simple maxima and minima and by computation of the standard deviations of the various quantities measured with the many short time-sections that make up the ensemble. Both methods are used to report results.

At much lower Reynolds numbers ( $Re < 10^3$ ) some variability has been attributed to different vortex shedding modes and wake instabilities that depend on the cylinder's true reduced velocity and the response amplitude. Williamson and Roshko (1988) and Morse and Williamson (2009a,b) contain very detailed investigations and descriptions of these phenomena. For high mass-ratio cylinders, Morse and Williamson (2010) showed that the response variability is associated with transitions between the possible vortex shedding modes in the wake. For very low mass-ratio cylinders like the one used in this investigation the situation is more complicated and the exact mechanisms leading to the response variability are not fully understood. It is not yet known if the same vortex shedding modes which were identified at the very low subcritical Reynolds numbers will survive at supercritical Reynolds numbers. Although the terms subcritical and supercritical Reynolds numbers are strictly defined for stationary (*i.e.* non-vibrating) cylinders. These terms are used throughout this paper to refer to the expected behavioral zones as a function of Reynolds number for both fixed and oscillating cylinders.

### 3. Test facility and experimental setup

All the experiments were performed in a 200 m long towing tank operated by the National Research Council (Ocean, Coastal & River Engineering) in St. John's, Newfoundland, Canada. The tank is 12 m wide and 7 m deep and is traversed by a 90 ton carriage with a maximum speed of 10 m/s. It is under this carriage that the VIV testing apparatus is mounted. The towing tank contained fresh water and its temperature was routinely checked every few hours. The water temperature was within the range of 15.8 to 16.0 degrees Celsius and the analysis in this paper uses a single value for the kinematic viscosity of water,  $\nu$ , equal to  $\sim 1.1 \times 10^{-6}$  m<sup>2</sup>/s.

The VIV testing apparatus consists of a collection of vertical and horizontal struts onto which a 0.325 m diameter by 6.233 m long aluminum pipe is mounted and is towed horizontally through the water. The test cylinder has an aspect ratio of  $\sim 19.2$  and has tear-drop shaped end plates to further minimize end effects. The relevant details for the spring-mounted cylinder are summarized in Table 1. The static equilibrium position of the pipe is 2 m below the free surface and is free to pivot behind two 3.0 m long tow bars. These two tow bars connect to the forward actuated struts which are on a closed-loop control and can closely follow the response of the freely vibrating cylinder so as to minimize the small arc that the cylinder would otherwise have to traverse.



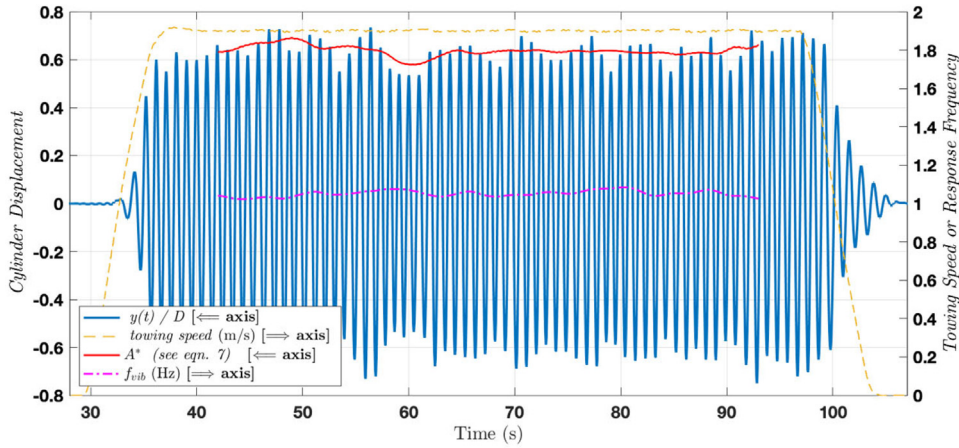


**Fig. 4.** A time-series from a conventional test with considerable variability in the response amplitude, test with stiff springs ( $f_n \sim 0.90$  Hz) &  $\zeta \sim 0.09$  at  $U \sim 1.9$  m/s ( $Re = 5.6 \times 10^5$ ) which corresponds to  $V_{Rn} \sim 6.5$ . (For interpretation of the references to color in this figure legend, the reader is referred to the web version of this article.)

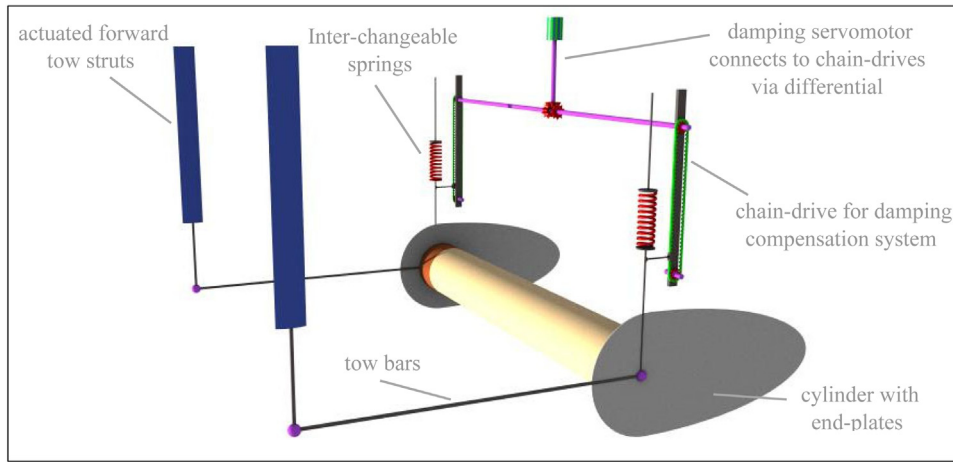


**Fig. 5.** Simplified schematic showing the 6.2 m long riser model and the connections between the forward and rear struts that are mounted beneath the towing-carriage. (For interpretation of the references to color in this figure legend, the reader is referred to the web version of this article.)

The pipe is supported on an internal tubular steel backbone via multiple load cells located at each end of the pipe. These load cells are used to create a five-component force dynamometer that can measure the cross-flow and in-line forces on either side. The quantity of trapped water is minimized but not entirely eliminated by the use of low-density foam between the steel backbone and the cylinder. These load cell measurements are not the main focus of this work and were primarily used for computing the in-line drag coefficients. For some select cases, the cross-flow excitation coefficients that were in phase with the cylinder velocity or acceleration were computed from the load cell measured forces and these were compared to the coefficients computed using Eqs. (4) & (5). These are discussed briefly in Section 4.4.

This steel backbone is supported via two vertical struts (rear struts) which pierce the free surface and prevent rolling motion. These rear struts are in-turn supported by a series of helical springs. The natural frequency of the oscillating components can be controlled by careful selection of the spring constant. Combinations of up to eight springs allow the total stiffness to be varied from 6 to 160 kN/m in about 20 increments. In this investigation tests were conducted with total spring stiffnesses of 23.58 kN/m and 40.28 kN/m. The oscillating cylinder and struts are also connected to a servo-motor (damping actuator) via chain drives and a differential. This servo-motor has traditionally been used as a damping compensation system injecting some energy back into the system in order to compensate for the mechanical damping present. In most of the tests described in this investigation the servo-motor was used in the opposite of its originally intended function. It was modified to add additional damping to the system, in a manner which will be described in greater detail later. Fig. 5 shows a simplified schematic of the spring-mounted cylinder and key components of the VIV testing apparatus.

**Table 1**

Riser model/Test cylinder properties.

Cylinder diameter	0.325 m
Cylinder length	6.233 m
Aspect ratio	~ 19.2
Dynamometer length (section of cylinder where forces are measured with internal load cells)	5.896 m
Oscillating mass (cylinder, flood water, struts & contributions from attached motors and bearings)	817 kg (approx.)
Mass of displaced water (for $C_m = 1$ in still water)	525 kg
Mass ratio	~1.56
Roughness ( $k_s/D$ )	~0.002
Stiffness (Soft Springs)	23.58 kN/m
Stiffness (Stiff Springs)	40.28 kN/m

The VIV testing apparatus was originally designed and developed by Don Spencer of the Oceanic Consulting Co. (OCC) for the DeepStar Joint Industry Project, Panel 5402 and allows for extensive configuration to suit specific investigation needs. During 2001–2003, OCC conducted an extensive research program for the DeepStar Consortium, including both free and forced oscillation experiments and explored the effects of roughness, turbulence and inline motion. [Spencer \(2004\)](#) contains a very detailed description of the experimental apparatus and some of the original DeepStar sponsored results have been made available to the public via the VIV data repository ([DeepStar, 2003](#)). Both [Dahl et al. \(2010\)](#) and [Constantinides et al. \(2013\)](#) also include good concise descriptions of the experimental system but in each case the test-rig was used in a slightly different configuration to accommodate their specific investigation objectives.

In the present experimental study, the apparatus was limited to purely cross-flow *free-response* VIV (*i.e.* in-line motion was restricted). The cylinder was never forced or given a prescribed motion, instead it was always free to respond to the incoming flow. Furthermore, the damping servo-motor was not used to pump energy into the system which is typically done in an attempt to ‘cancel-out’ the inherent mechanical damping present. Instead, for most tests it was disconnected from the power-supply/controller and large resistors were connected across the motor’s input terminals. The electric motor then functioned as a generator. Varying the connected resistance varied the damping that the motor applied to the mechanical system in a very predictable way. Lower resistance values gave rise to higher effective mechanical damping due to large counter EMF. [Fig. 6](#) shows the plot of resistance versus equivalent mechanical damping constant measured from many *free-decay* tests.

The riser model included a very thin roughness jacket that completely covered the aluminum cylinder and was necessary because the range of Reynolds numbers that would be tested in this campaign falls exactly in the ‘drag crisis’ regime of very smooth surfaced cylinders. The rough surface was created by gluing fine grit on a thin polymer sleeve covering the cylinder. The resulting surface roughness employed was on the order of  $k_s/D \sim 2 \times 10^{-3}$ . When installed, the roughness jacket helps trip the boundary layer separation at much lower Reynolds numbers, with the fixed cylinder ‘drag crisis’ occurring in the neighborhood of  $Re \sim 10^5$ .

The first round of experiments described in this paper were performed between March 2nd–4th, 2015, and the second round was completed on December 8th, 2015. The experiments were conducted under contract with Oceanic Consulting Co. and the authors were present during commissioning and testing and were entirely responsible for the design of the test matrix, for all the modifications to the damping system and for programming the carriage controller to achieve the desired ramp profiles.

The first round of testing completed included two different springs constants (23.58 kN/m and 40.28 kN/m) and the cylinder’s response was measured over two Reynolds number ranges ( $2.4 \times 10^5 < Re < 6 \times 10^5$  and  $3 \times 10^5 < Re < 7 \times 10^5$  respectively). After analyzing the data collected in the first round it was determined that even more damping was needed to be able to obtain a complete lift coefficient map. The primary goal of the first round of tests was to demonstrate that *free-response* VIV tests using slowly varying towing speeds was a viable high Reynolds number testing technique. Additionally, the response information collected at the two different supercritical Reynolds numbers would reveal whether Reynolds effects exist in the supercritical region. With the opportunity to conduct a second round of tests in December 2015, the goal of the test was broadened to obtain complete coefficient maps for lift and added mass that could be used for VIV prediction at supercritical Reynolds numbers.

Each round of testing included *pluck* or *decay* tests in still water, *free-response* VIV tests and *fixed cylinder drag* tests.

In the *fixed cylinder drag* tests, the riser model is held fixed while it is towed through the towing tank. Experiments were performed at both steady and constantly varying towing speeds. The goal of these tests was to measure the drag loads and to calculate drag coefficients for fixed (*i.e.* stationary) cylinders over a large range of Reynolds numbers which could then be compared with the drag coefficients of the freely vibrating cylinder. The very small variation in the measured drag coefficient that was observed from  $2 \times 10^5 < Re < 1 \times 10^6$  when contrasted to the large variation that was observed when the Reynolds number was lower ( $Re < 1 \times 10^5$ ) proves that Reynolds numbers larger than approx.  $2 \times 10^5$  correspond to the supercritical Reynolds number regime for the roughened cylinder tested used in this investigation. These results are discussed in detail in [Appendix A](#).

In the *free-response* or *free-vibration* VIV tests, the riser model is mounted on springs and is free to respond in the cross-flow direction to the hydrodynamic forces while towed through the tank. Experiments were performed at both steady

and continuously varying towing speeds. The objective was to measure the response amplitude and response frequency. The response information could then be combined with the system properties (mass, stiffness and varying damping) to compute the lift and added mass coefficients. Tests were conducted with two different spring stiffnesses and hence the peak VIV response occurred for two different Reynolds number ranges. The goal was to compare the response information and the computed excitation coefficients at these two different Reynolds number ranges and thus determine whether any Reynolds effects exist in what would correspond to the fixed-cylinder supercritical Reynolds regime. These tests and the computed coefficients are the main focus of this paper and are presented in Section 4.

In *pluck* or *decay tests* the riser model is mounted on springs and is given an initial displacement (pluck) while the towing carriage is stationary. These tests are only performed while the carriage is stationary and the primary goal is to measure the natural period and damping present for a particular combination of spring constant and damping setting. The amount of damping was modified by connecting different electrical resistors to a servo-motor which had been traditionally used as a damping compensation system. All such tests were performed with the cylinder submerged in still water (*i.e.* still water tests). These results are discussed here only briefly since the analysis techniques are well known and established in the field of structural dynamics.

The VIV testing apparatus that is mounted beneath the tank's towing carriage has a significant amount of mechanical damping due to bearings, sliding friction and gear friction. In previous tests Oceanic Consulting Corp. staff used a damping compensation system to cancel out this non-negligible amount of mechanical damping. In this work instead of pumping energy into the riser model by supplying power to the damping compensation servo-motor it was necessary to determine a way by which the same servo-motor could be used to dissipate energy. This was achieved by disconnecting the power supply to the servo-motor and instead connecting electrical resistors across the servo-motor's terminals in order to dissipate large amounts of energy. The servo-motor was thus used as a generator. The equivalent damping constant was varied by varying the resistance connected to the terminals of the servomotor. The electro-mechanical damping introduced was measured by conducting a number of 'pluck tests' (*i.e.* free-decay tests with initial displacement) for each spring/damper combination. For most combinations of springs and electro-mechanical damping these tests were repeated multiple times.

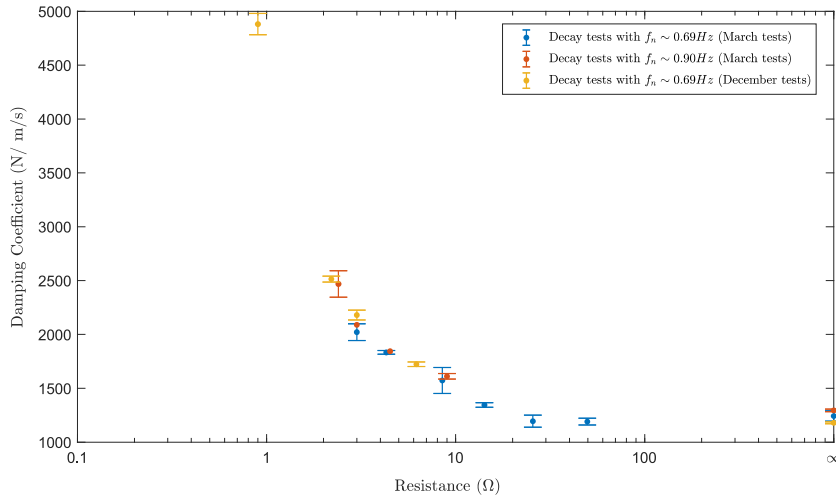
The system's response to the initial condition occurs at the damped natural frequency and the decay rate provides an estimate of the damping ratio and logarithmic decrement. The undamped natural frequency and the equivalent linear damping coefficient can then be readily computed from the known relations. The damped natural frequency was calculated using the zero-crossing method and the damping ratio was determined both by the log-decrement method and by fitting decaying exponentials to the signal envelope. The damping ratio calculated using both of these methods produced very similar results. The damping measured in the still water decay tests included at least three sources: all the mechanical linkages in the testing apparatus; the electro-mechanical damping from the energy dissipated in the attached resistors; and a small amount of still-water damping; all of which contribute to the measured values. The total oscillating mass was always computed based on the measured natural frequency and an estimate of the still-water added mass using  $C_M = 1.0$ . This was determined to be the most reliable method for accounting for the inertia of all the oscillating linkages and rotating components connected to the main test cylinder.

Fig. 6 summarizes the results from all the decay tests performed. The plot shows the calculated damping coefficient as a function of the resistor value that was connected to the terminals of the damping servo-motor. When pluck tests for spring and damping combinations were repeated enough times to gather some meaningful statistics, the uncertainty in the measured damping coefficient is shown with error-bars. In Fig. 6, infinite resistance is equivalent to an open circuit (*i.e.* no resistors connected to the servo-motor terminals). In this case there is no energy dissipated in the electrical resistors and the only damping present is due to the mechanical damping of the oscillating and rotating components (*e.g.* linkages, chain-drives, gears, differentials and servo-motor) and any still-water damping contributions.

Table 2 summarizes the results from the pluck tests conducted during both the March and December round of testing. The table only lists the damping values which were subsequently used for the free VIV tests (steady towing speed or ramp tests) whereas Fig. 6 includes some additional damping values that were tested while investigating the behavior of the system. The experimental uncertainty ( $\pm 1$  st. dev.) in the measured damping coefficient was typically between  $\pm 2\%$  and  $\pm 5\%$  of the measured damping value with one damping setting showing an uncertainty as large as  $\pm 8\%$ .

Since this was a brief, proof-of-concept test, conducted under very constrained time conditions, the damping measurements were the best obtainable under the circumstances. Future *free-response* VIV tests at this facility would benefit from improved damping measurements. Specifically, one would need to confirm that the damping present in the system is relatively amplitude independent or if it is found to be amplitude dependent one should try to carefully characterize that relationship. 'Pluck tests' were only performed using one initial displacement approximately equal to  $0.2D$  and thus it was not possible to fully characterize the amplitude dependence of the damping present in the system. Furthermore, it would be useful to quantify the hydrodynamic contribution in these still water tests so as to better separate the portion of damping due to the still water as opposed to damping in the actual mechanical setup. The analysis presented in this paper estimated the still-water damping contribution at approximately  $100 \text{ N/m/s}$  based on the still-water damping term in the hydrodynamic damping model developed by Venugopal (*eqn. 3.7* in Venugopal, 1996). The Venugopal still water model was derived from a curve fit to experimental data.

Fig. 6 shows that the damping coefficients measured for both spring stiffnesses in the March tests are in good agreement and these are further corroborated by the very good agreement of the repeated tests with the softer set



**Fig. 6.** Damping coefficient (N/m/s) vs. Resistance ( $\Omega$ ) as measured in the still-water pluck tests (free decay). (For interpretation of the references to color in this figure legend, the reader is referred to the web version of this article.)

**Table 2**  
Summary of free decay tests.

$f_n$ (Hz)	Resistor or damping setting	$\zeta$ (-)	$c_{measured}$ (N/m/s)	$c_{final}$ (N/m/s)
$0.90 \pm 0.01$ (40.28 kN/m stiffness – March 2015)	No resistor connected	0.09	$1295 \pm 12$	1114
	9 $\Omega$	0.11	$1611 \pm 26$	1393
	4.5 $\Omega$	0.13	1844	1722
	3 $\Omega$	0.15	2090	2033
$0.69 \pm 0.01$ (23.58 kN/m stiffness – March 2015)	No resistor connected	0.11	$1243 \pm 48$	1114
	8.6 $\Omega$	0.15	$1573 \pm 121$	1393
	4.3 $\Omega$	0.17	$1833 \pm 17$	1722
	3 $\Omega$	0.19	$2021 \pm 78$	2033
$0.69 \pm 0.03$ (23.58 kN/m stiffness – December 2015)	Damp. Compensation ON	$\sim 0.0$	0	0
	Damp. Compensation ON	0.03	$348 \pm 12$	248
	No resistor connected	0.10	$1179 \pm 9$	1114
	6.2 $\Omega$	0.16	$1723 \pm 21$	1514
	3 $\Omega$	0.20	$2180 \pm 46$	2033
	2.2 $\Omega$	0.23	$2514 \pm 28$	2425
	0.9 $\Omega$	0.49	$4881 \pm 99$	4765

of springs in the December tests. The final damping coefficient for each spring–damper combination that was used for calculations of  $c^*$  and  $C_L$  was obtained after curve fitting all available free-decay data from both testing campaigns and subtracting the computed still-water damping contribution. The damping coefficients that result after fitting all the available measured data are listed in the last column of Table 2. These are the damping coefficients that were used for computing  $c^*$  from the measured response quantities in the *free-response* VIV towing tests. For the two damping settings of  $\zeta \sim 0.00$  &  $\zeta \sim 0.03$  which utilized the damping compensation system in its original intended form, curve fitting was not used.

## 4. Results and discussion

### 4.1. Comparison of ramp tests with steady tests

Several of the *free-response* VIV tests described in this paper were performed at constant towing speed. This was done to obtain a few reference values against which the variable towing speed test results could be compared. The comparisons focused on the response amplitude and response frequency as a function of the reduced velocity. Great effort was made to ensure that the towing speed was varied slowly enough. The  $\gamma$  value rarely exceeded 0.02 and was usually closer to 0.01 for most ramp tests which corresponds to approximately a 1% change in towing speed per cycle of vibration.

The response amplitude,  $A^*$ , is defined as:

$$A^* = \frac{\sqrt{2} Y_{RMS}(t)}{D} = \frac{\sqrt{2}}{D} \sqrt{\frac{1}{5T_n} \int_{-2.5T_n}^{2.5T_n} (y(t))^2 dt} \quad (7)$$

where  $Y_{RMS}(t)$  is the ‘moving RMS’ of the cylinder’s displacement in the cross-flow direction,  $y(t)$ , computed from within a moving-window 5 cycles long. The maximum amount of overlap was used with adjacent windows being offset from each other by just one discrete sample. This estimate of the amplitude can be seen and compared to the actual displacement time-series in Figs. 2–4. Using the exact vibration period, which does changes slightly during a ramp test, instead of the natural period, to determine the width of the moving-window led to insignificant differences in the computed statistical quantities. All response amplitudes reported in this investigation are the result of using Eq. (7) on the instantaneous cylinder displacement  $y(t)$ . The displacement itself was computed by double-integrating the accelerations measured on either side of the cylinder. The resulting displacement estimates were checked against the displacement measured by a single ‘yo-yo’ potentiometer attached to one side of the cylinder.

The (nominal) reduced velocity,  $V_{R_n}$ , is defined as:

$$V_{R_n} = \frac{\bar{U}(t)}{D f_n} \quad (8)$$

and is based upon the measured still-water natural frequency,  $f_n$ , and the mean towing velocity,  $\bar{U}(t)$ , computed from within a moving-window 5 cycles long.

The (true) reduced velocity,  $V_{R_{vib}}$ , is defined as:

$$V_{R_{vib}} = \frac{\bar{U}(t)}{D f_{vib}(t)} \quad (9)$$

and is based upon the mean response frequency,  $f_{vib}(t)$ , and the mean towing velocity,  $\bar{U}(t)$ , both of which are computed from within a moving window that is  $\sim 5$  cycles long. In this investigation, the instantaneous response frequency,  $f_{vib}^{inst}(t)$ , was computed using the Hilbert transform on the directly measured accelerometer signals. The mean response frequency as a function of time,  $f_{vib}(t)$ , was then computed using a moving-window 5 cycles long in order to be consistent with the other response quantities reported.

The Reynolds Number,  $Re$ , is defined as:

$$Re = \frac{\bar{U}(t) D}{\nu} \quad (10)$$

Fig. 7 shows the VIV response amplitude and frequency as a function of nominal reduced velocity for the tests with a damping of  $\zeta \sim 0.09$  and with the stiffer spring constant of 40.28 kN/m. These data are at the highest Reynolds number tested in the *free-response* cylinder arrangement. In these tests the low mass-ratio of the cylinder resulted in a very wide synchronous response region and equipment limitations did not allow extending the tests into the desynchronization region. The figures compare the response parameters extracted from the ramp tests with the response parameters measured in several constant speed tests. Given the good agreement that exists for the majority of the comparisons shown between ramp tests and steady tests, the authors believe that properly and carefully executed ramp tests can form suitable alternatives to traditional constant speed testing. This is especially true after one takes into consideration the response variability that exists in both the steady towing speed tests and the time-varying flow tests.

Results extracted from accelerating ramp tests are plotted with a blue line and results from decelerating ramp tests are plotted in green lines. Note that the two increasing or decreasing ramp tests did not have the exact same starting and ending towing speeds. The variability that is observed in the constant speed tests is indicated by a vertical red bar, which reveals the range of the measurements from the minimum observed value to the maximum. The values were computed using a 5 cycle long moving-window, which was swept through the entire time-series for each constant speed test with the largest amount of overlap possible. A short vertical red line reveals a test speed at which there was little response variability, as shown in Fig. 3 for  $V_{R_n} \sim 5.5$ . By contrast a tall vertical red line indicates significant response variability, as revealed in Fig. 4 at  $V_{R_n} \sim 6.5$ .

The greatest limitation of a ‘ramp test’ is that the cylinder responds at each flow condition for a limited number of cycles. As a result, when the cylinder is being tested in conditions that result in unsteady response which is associated with amplitude and frequency modulations, the response data collected from that short time-window represents just one realization from the range of the possible responses. Repeated ramp tests are necessary to properly characterize the possible response variability. This would have been especially important if strong and distinct bistable response behavior had been observed in the steady test runs, which was never the case for the limited number of steady tests conducted. A repeated ramp test will not always yield identical results at a specific reduced velocity value. In regions where the response variability is small, the result from repeated accelerating ramp tests (or decelerating ramps tests) will be in close agreement. Conversely, in reduced velocity regions where the response variability is large there will be greater variation in the results from repeated ramp tests. For example, at the reduced velocity corresponding to peak response ( $V_{R_n} \sim 5.5$ ) there is very little variability in amplitude and frequency. This is observed in both accelerating and decelerating flows and is consistent with the small variation that is seen in the constant speed tests with low damping values at the same reduced velocity. Similarly, the response data collected from the various repeated ramp tests at  $V_{R_n} \sim 6.5$  showed a larger range of possible values which is consistent with the large variability seen in the corresponding steady speed test. It is good practice to repeat ramp tests and use the results from the repeated tests to compute a mean and standard



deviation of the response metrics at each value of  $V_{Rn}$ . This provides an estimate of  $A^*(V_{Rn})$  and  $f_{vib}(V_{Rn})$ . These can then be compared to the mean and standard deviation observed in the constant speed tests. The data that was gathered show that the results of the ramp tests are in close agreement with the constant speed tests. Furthermore, ramp tests are able to quickly reveal significant response characteristics over a smoothly and continuously varying range of flow speeds.

One particularly interesting feature in the VIV response data shown in Fig. 7 is the 'hysteresis' that occurs for  $\sim 4.3 < V_{Rn} < \sim 5.2$ , when one compares the response from accelerating ramp tests (blue lines) to the response extracted from the decelerating ramp tests (green lines). This illustrates that increasing or decreasing the flow speed during tests affects the observed VIV response and hence the flow history matters in certain regions of reduced velocity. Careful examination of the figures reveals that the difference observed in the response amplitude is associated with a small difference in the response frequency, with the cylinder choosing to respond at frequency that is consistent with its prior history in each case. There is a second region between  $\sim 6.5 < V_{Rn} < \sim 7.5$  that may also show some signs of hysteresis which are especially evident when comparing the response frequency for the decreasing or increasing ramps in that region. The first identified hysteresis region for this damping setting coincides with the jump from the 'initial branch' to the 'upper branch' and is very repeatable whereas the second appears to correspond to the transition from the 'upper branch' to the 'lower branch' and is more stochastic in nature. Finally, it is interesting to note that the steady test results are in closer agreement with the increasing ramp test results (i.e. slowly accelerating flows) rather than the decreasing ramp test results (i.e. decelerating flows). This of course is to be expected since the steady towing speeds in this investigation were always attained by a towing carriage starting from zero speed.

Hysteresis is a well-known VIV effect but can easily be overlooked in conventional constant speed tests unless great care is taken to provide the system with the appropriate initial conditions or great care is taken to approach the desired steady testing speed from an intentionally higher or lower speed. A well-executed accelerating ramp test followed by a decelerating ramp test can easily reveal these hysteresis effects in just two runs down the tank. Bishop and Hassan (1964) first showed that the hysteresis is associated with a sudden jump in the phase between the excitation force and the cylinder response. Williamson and Roshko (1988) later used careful flow visualization experiments to attribute the differences observed in the hysteresis region to a change in the vortex shedding pattern from a '2S' pattern (two single vortices shed per oscillation) to a '2P' pattern (two pairs of vortices shed per oscillation) that happens very suddenly as a result of very small and subtle changes in the cylinder's oscillation amplitude and reduced velocity. Both Govardhan and Williamson (2000) and Morse and Williamson (2009a) contain excellent reviews of the various vortex shedding modes that exist at low subcritical Reynolds numbers. If the observations regarding the vortex shedding modes and the transitions from one response branch to another that were made at those low Reynolds numbers are still relevant to the VIV at supercritical Reynolds numbers, then the first 'hysteretic' region that was discussed earlier could be the result of a switching between the '2S' to the '2P' or the '2P<sub>overlap</sub>' (2P<sub>o</sub>) modes and vice-versa.

The response variability observed for the steady test at  $V_{Rn} \sim 6.5$  which is demonstrated by the long vertical bar and the slight response variability observed in the different repeated ramp results between  $5.5 < V_{Rn} < 7.5$  could likely be attributed to the intermittent switching between the '2P' and '2P<sub>o</sub>' modes. Based on their analytical response models, Morse and Williamson (2010) classify this reduced velocity region VIV as the 'unsteady' VIV region for low mass ratio cylinders. Appendix B shows that all the response information for the nominal reduced velocity range of  $5.5 < V_{Rn} < 7.5$  folds onto itself at a true reduced velocity of  $V_{vib} < \sim 5.5$ . This puts all the response data right on the cusp of the '2S', '2P' and '2P<sub>o</sub>' vortex shedding modes discussed in Morse and Williamson (2009a).

Because the literature does not include readily available studies of systematic flow visualization for vibrating cylinders at supercritical Reynolds numbers, it is impossible to say conclusively whether the observed response variability or unsteadiness is due to transitions between the vortex shedding modes which are known to occur at very low Reynolds numbers or there are more general variations in the spanwise coherence of the shed vortices at these supercritical Reynolds numbers. Given that the existing low subcritical Reynolds number testing and literature clearly associates the transition between the '2P' and '2S' wake patterns with a hysteretic response, then it is reasonable to believe that second hysteretic region that is occasionally observed is also associated with a transition to and from the '2P' and '2P<sub>o</sub>' wake states. It is likely that this second hysteresis and the associated wake transitions are a very intermittent or a random effect that do not occur as strongly and repeatedly as the strong hysteresis observed between the '2S' and '2P' regions. Only after careful wake visualization studies are completed at these supercritical Reynolds numbers will this be determined definitively.

In a similar manner to what was shown in Fig. 7 the response parameters observed from ramp tests for all combinations of spring stiffness and damping were compared to the results from steady tests and in most situations, the authors believe that the agreement was satisfactory and sufficient for the purposes of computing coefficient surfaces. During the testing conducted in March 2015, more than 50 ramp tests and 40 steady tests were conducted at multiple spring and damping combinations to confirm that well designed ramp tests are suitable alternatives to many individual steady towing speed tests.<sup>1</sup> If a ramp test was started with a reduced velocity in the range of  $4.5 < V_{Rn} < 5$  (i.e. inside the region that shows

<sup>1</sup> All the detailed comparisons between the steady tests and the ramp tests from the 1st round of testing in March 2015 are described in the original technical report that was prepared at that time (Vandiver and Resvanis, 2015). In that report the soft-spring cases corresponding to the lower Reynolds number range are referred to as having a still-water natural frequency of 0.75 Hz instead of the value of 0.69 Hz which is listed in this manuscript. The difference arose after revisiting the data and recomputing natural frequencies from the first round of pluck tests. When the measured period is based on the first few response cycles of the transient decay and while the amplitudes are non-negligible, the added mass coefficient is larger and one obtains a still water natural frequency estimate of 0.69 Hz. This result is used in this paper.

the strong hysteresis effect) instead of the region immediately before the strong hysteresis at approximately  $3.5 < V_{Rn} < 4$  which was more often the case for the ramp tests conducted, it was found that the recorded response amplitudes in that region could occasionally be some 10%–15% lower than expected from steady tests. The small number of ramp tests that was started inside the strong hysteresis region was excluded from the data shown in this investigation. This peculiar behavior is most likely due to strong hysteresis effects that exist in that region and strongly suggests that an increasing speed ramp test should begin at towing speeds before the hysteretic region.

The comparisons between the steady tests and the ramp test results revealed that as long as the  $\gamma$  parameter is kept low in these slowly accelerating or decelerating flows, the cylinder has sufficient time to respond to gradually changing hydrodynamic loads in a manner that is similar to what is observed in steady tests. Differences between the response in steady flows and slowly accelerating or decelerating flows tend to be limited to regions where either strong hysteresis effects exist or regions that show large response variability even for steady testing. The cause for this response variability at supercritical Reynolds numbers is not yet known. The comparisons of the response quantities in steady and time-varying flows are shown in a concise manner in the following section. That section focuses on demonstrating how the *free-response* VIV information from multiple damping values can be used to compute added mass and lift coefficient surfaces from *free-response* VIV.

In a typical ramp test the towing speed,  $U$ , the dimensionless response amplitude,  $A^*$  and the response frequency,  $f_{vib}$ , vary in time as a result of the changing reduced velocity, which implies that the lift coefficient and added mass coefficients will also vary in time during each test. The response quantities measured in a *free-response* VIV test, when combined with knowledge of the mass, stiffness and damping present in the system, are sufficient to compute the lift and added mass coefficients according to Eqs. (4) & (5). For a given run down the tank the damping coefficient has been set beforehand. Therefore, one simply needs to measure and record the cylinder's displacement,  $y(t)$ , and response frequency,  $f_{vib}(t)$ , as a function of towing speed,  $U(t)$ , in order to be able to compute both excitation coefficients. Finally, compiling a complete lift coefficient and added mass coefficient surface ( $C_L$  or  $C_M$  vs.  $A/D$  vs.  $V_{Rn}$ ) simply becomes an exercise of repeating *free-response* VIV tests for several values of damping as will be demonstrated in the following section.

If one has the luxury of repeating a given ramp test several times, then the recorded response quantities at each value of reduced velocity can be averaged leading to considerably smoother response curves and excitation coefficient surfaces that are less affected by the inherent response variability. Clearly, the approach of obtaining hydrodynamic coefficients from response data and the governing equations is also applicable to the results obtained in traditional steady speed tests but many more tests are necessary in order to sufficiently cover the reduced velocity parameter space and obtain a sufficient number of data points to fit the coefficient surfaces. At this facility, the entire range of reduced velocities ( $V_{Rn}$ ) that were of interest could easily be covered with a single well-designed ramp test. Additional ramp tests can be repeated and the information can then be used to characterize the inherent response variability that exists at high Reynolds numbers.

#### 4.2. Hydrodynamic coefficients from free-response VIV data (March tests)

Fig. 8 demonstrates the effect of increasing damping on the VIV response amplitude and response frequency for the four damping values tested with the stiffer 40.28 kN/m springs. The response amplitudes measured when using these stiff springs represent the highest Reynolds number results obtained during the *free-response* VIV tests. These data are used to compute the added mass and lift coefficient surfaces at the higher of the two supercritical Reynolds number ranges reported in this investigation.

Instead of plotting the results from all the individual ramp tests for each damping setting, Fig. 8 shows the mean values of the recorded response quantities at each red. velocity value for each damping setting. Therefore, the multiple curves that were shown in Fig. 7 for  $\zeta \sim 0.09$  are now replaced by just a single line. At each damping level, the variability between repeated ramp tests is now demonstrated by the shaded regions which correspond to  $\pm 1$  standard deviation (st. dev.) around the mean value of response amplitude or response frequency at each reduced velocity value. The portions of the curve which have small or negligible shaded regions indicate that values obtained from repeated ramp tests were in close agreement at that value of reduced velocity, whereas the large shaded regions indicate greater differences between repeated ramp tests and indicate greater response variability. The shaded regions are observed to be larger in the region of the transition from the initial to upper branch since both increasing and decreasing ramps have been used to compute the statistics for  $\pm 1$  st. dev. and this is the region where strong hysteresis effects are known to exist.

The constant towing speed test results for each damping setting are shown as individual data points with error bars extending to  $\pm 1$  st. dev. of the quantities of interest after going through the entire time-series with a moving window. No steady tests were conducted for  $\zeta \sim 0.15$  and that is the reason why no data points are shown for that setting in the figures. The figure includes detailed views to further facilitate the comparison of the ramp test results with the steady test results for the portions of the plot that are crowded. The comparison of the ramp test results with the steady test results shows that the cylinder response in these very slowly time-varying flows is similar to the response in steady flows. After the response variability which is shown as error bars for the steady tests and shaded regions for the ramp tests is taken into account, the agreement is close for all comparisons except for two results for the  $\zeta \sim 0.11$  ramp results which are shown in detail. The first is at  $V_{Rn} \sim 4.5$  which is approximately 10% larger than the steady test result and the second poor comparison is at  $V_{Rn} \sim 7.5$  where the ramp test result is approximately 10% smaller. The first of these reduced velocity values corresponds to the region where strong hysteresis effects exist whereas the second region is associated

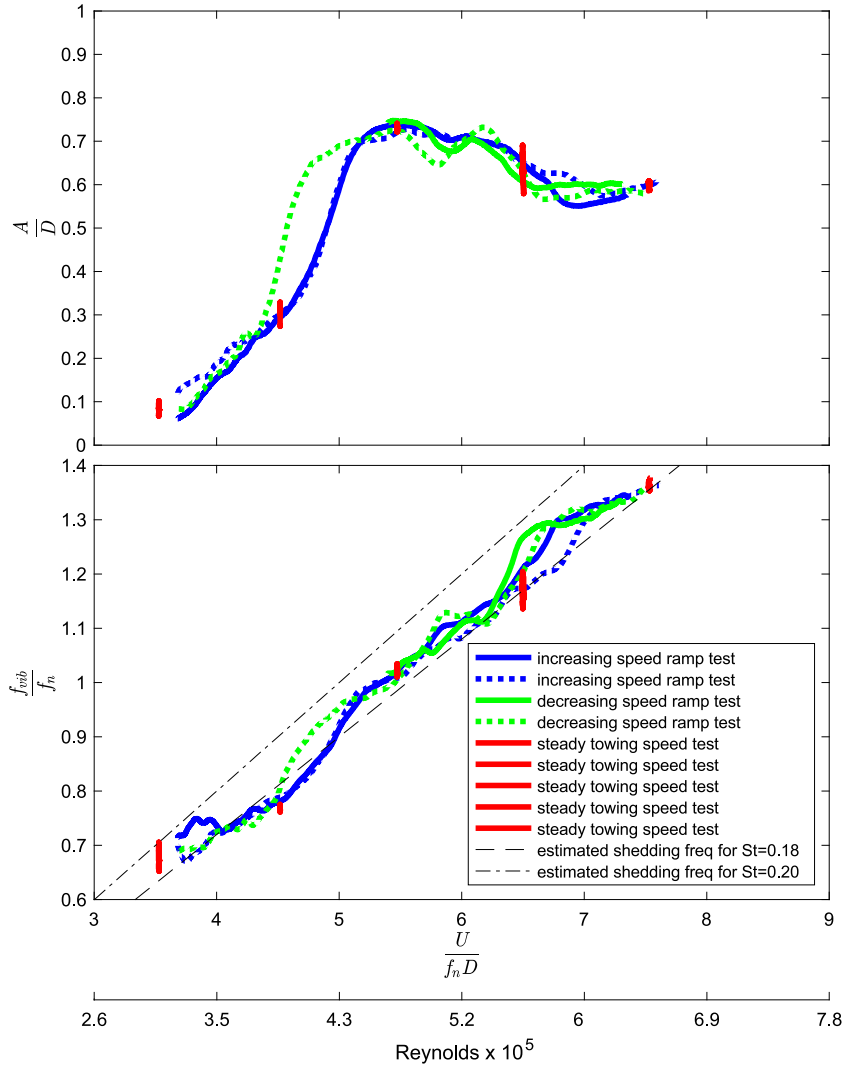


**Fig. 7.** Dimensionless response amplitude (TOP) & dimensionless response frequency (BOTTOM) vs. reduced velocity or Reynolds number for tests with stiff springs ( $f_n \sim 0.90$  Hz) and  $\zeta = 0.09$ . (For interpretation of the references to color in this figure legend, the reader is referred to the web version of this article.)

with larger response variability. It is especially important to point out that the peak response amplitudes at  $V_{Rn} \sim 5.5$  are captured well by the ramp tests since it is the comparison of the peak response amplitude at different Reynolds numbers that will reveal if there are strong or weak Reynolds number effects in the supercritical region. Additionally, it is peak response at a given damping level that most concerns the designers of full-scale engineering structures in the ocean.

Fig. 9 shows contours of lift coefficient and added mass against response amplitude and reduced velocity computed using all the accelerating ramp test results when the 40.28 kN/m springs were installed on the testing rig. The lift and added mass coefficients were computed using Eqs. (4) & (5) as discussed earlier. The coefficient surfaces are only shown in regions where response amplitude information was available. The largest lift coefficient computed had an approximate value of 0.77 and occurred at  $V_{Rn} \sim 5.4$  &  $A/D \sim 0.55$  when the Reynolds number was  $\sim 4.95 \times 10^5$ . The maximum lift coefficient remains virtually unchanged at 0.78 and occurs at  $V_{Rn} \sim 5.4$  &  $A/D \sim 0.56$  if both accelerating and decelerating ramp tests are used to create the lift coefficient surfaces.

Fig. 10 demonstrates the effect of damping on the VIV response amplitude for four different damping values that were tested when the softer 23.58 kN/m springs were installed. The softer springs and hence lower natural frequency move the synchronization region to a lower Reynolds number range when compared to the stiffer springs presented earlier in Fig. 8. The recorded response amplitude and response frequencies at these four damping settings were used to compute the added mass and lift coefficient surface at the lower of the two supercritical Reynolds number ranges that were tested in this investigation. The solid lines represent the mean value for the response quantity at each reduced velocity value after

performing repeated accelerating or decelerating ramp tests. The response variability that was observed in the response amplitude or response frequency is shown by the shaded regions which represent  $\pm 1$  st. dev. around the mean values. Similarly, the error bars around the steady towing speed results demonstrate the response variability that exists even in steady tests by showing  $\pm 1$  st. dev. of the quantities of interest after passing through the entire time-series with a moving window. The conclusions from the comparisons of the steady tests and the ramp tests at the lower Reynolds number follow the conclusions drawn earlier from the discussion of Fig. 8. The largest differences occur in regions where hysteresis effects are greatest.

Both the response amplitude and the frequency observed in these slowly-time varying flows is close to what is observed in the constant speed tests with the most significant differences limited to just one set of tests with a particular spring-damper combination. The ramp results when the cylinder had the largest amount of damping  $\zeta \sim 0.19$  show the least favorable comparison between steady and time-varying flow results but there is still complete overlap after the response variability is taken into account. This is because the decelerating ramp tests systematically had lower response values for  $V_{Rn} > 6$ , with their response results being up to 20% smaller than the increasing ramp results for this damping value. This represents the largest difference observed between the increasing and decreasing ramp tests. Both increasing and decreasing ramp tests showed the greatest response variability in this region and both of these reasons contribute to the large extent of the shaded region. A similar behavior but with less dramatic differences was observed for the tests with the largest amount of damping and the stiffer springs ( $\zeta \sim 15\%$ ) shown earlier in Fig. 8. The steady towing speeds were always approached from standing (i.e. from a lower speed) and therefore their results do not compare as favorably with the compounded ramp tests results that include data from both accelerating and decelerating flows. The steady test results overlap and are closer to the upper bounds of the shaded region that is primarily dictated by the data collected in the increasing speed tests. The response amplitudes recorded for the  $\zeta \sim 0.19$  damping tests are quite moderate with values of  $0.4\text{--}0.5D$  and occur over the range of  $5.4 < V_{Rn} < 8$  which corresponds to true reduced velocities of  $5.8 < V_{Rvib} < 6.3$ . These amplitudes and true-reduced velocities place this section of the *free-response* curve right on the boundary of the '2S' and '2P' and the lower extent of the '2P<sub>o</sub>' vortex shedding modes identified in very low Reynolds number tests. As emphasized earlier, without flow visualization it is not possible to know if the same wake behaviors exist at supercritical Reynolds numbers and hence hysteresis effects are responsible for the behavior observed in these tests or whether the response variability is due to some other factors like more general fluctuations in the spanwise coherence of the shed vortices.

With the exception of the reduced velocity range between  $\sim 4.5 < V_{Rn} < \sim 5.5$  where it is known that the response variability is caused by hysteresis and the very noticeable and repeatable differences between increasing and decreasing speed tests, further investigation and testing is necessary to properly characterize the response variability at other reduced velocity values. This is especially true for the largest damping settings used in this investigation. It would be particularly interesting to understand why certain reduced velocity values and response amplitude combinations lead to larger response variability whereas others regions show little or no response variability. This would require many individual constant towing speed tests at closely spaced reduced velocity values or a large number of repeated ramp tests in order to obtain many individual yet short-duration realizations of the response at each value of reduced velocity. Ideally this would be complemented by careful flow visualization techniques to simultaneously study the behavior of the vortex shedding in the wake at these supercritical Reynolds numbers.

Fig. 11 shows contours of lift coefficient and added mass coefficient against the response amplitude and the reduced velocity computed using all the increasing speed ramp test results when the 23.58 kN/m springs were installed on the rig. The largest lift coefficient has an approximate value of 0.84 and occurs at  $V_{Rn} = 5.9$  &  $A/D = 0.62$  when the Reynolds number was  $\sim 3.8 \times 10^5$ . The coefficient surfaces computed for the 23.58 kN/m springs are more extensive than those shown previously for the 40.28 kN/m springs because as demonstrated in Fig. 10 some of the selected damping values resulted in smaller response amplitudes than what had been previously achieved with the stiffer springs. Additionally, for one of the damping and spring combinations, the programmed ramp profile was extended all the way to a  $V_{Rn}$  value of  $\sim 9$ . The maximum lift coefficient changes slightly to 0.86 and occurs at  $V_{Rn} = 5.55$  and  $A/D = 0.58$  if both accelerating and decelerating tests are used to compute the lift coefficient surfaces.

When creating these coefficient surfaces there is minimal need for interpolation in the  $V_{Rn}$  dimension because the ramp tests allowed the continuous extraction of response data as the towing speed and hence the  $V_{Rn}$  was being varied. In the  $A/D$  dimension, a small amount of interpolation was necessary to populate areas of the coefficient surfaces that lay between the response amplitudes recorded for each of the four values of damping. The areas where it was necessary to interpolate in the  $A/D$  dimension can easily be identified and approximated as the 'white-space' between the shaded areas in Figs. 8 and 10. The actual extent of interpolation necessary was even smaller since the shaded regions represent only  $\pm 1$  st. dev. around the mean values and not the full extent of the ramp results around the mean values.

These initial tests were successful in capturing the peak lift coefficient occurring at approximately  $V_{Rn} \sim 5.9$  and  $A/D \sim 0.62$  but further testing was necessary to populate the empty regions in the figures. Specifically, further testing needed to include several more damping values in order to obtain a more extensive  $C_L$  surface. Performing tests with larger amounts of damping (i.e. larger than  $\zeta \sim 19\%$ ) would help populate the  $C_L$  contours that are missing from the area labeled Region I in Fig. 11. Similarly, performing tests with smaller amounts of damping than those that were tested at the time (i.e. smaller than  $\zeta \sim 11\%$ ) would provide the necessary information for the area labeled Region II. Finally, it should be apparent that populating the area labeled Region III is not possible solely with this kind of *free-response* VIV tests

since these combinations of response amplitude and reduced velocity are not associated with self-excited vibrations. The boundary between *Regions II* and *III* is the area of little to zero lift contour and therefore the lift coefficient in *Region III* is negative and VIV are not excited unless there is an external force driving the system at that combination of inputs (i.e. not self-induced vibrations but rather *forced-vibration*). Note that to overcome these limitations, Blevins (2009) provided his elastically mounted cylinders with an initial displacement and would then release the system to observe the decay in the steady cross-flow. By repeating the test many times for different initial amplitudes and flume velocities he was able to populate the entire parameter space of  $A/D$  vs.  $V_{Rn}$  including the regions where *self-excited* VIV is not possible and lift coefficient values are negative.

As discussed earlier in the introduction, the goal was to measure and capture the region of peak lift coefficient and not to obtain the largest possible response amplitude which would correspond to the limit-cycle amplitude at zero or nearly zero lift coefficient. Acquiring the additional data for *Regions I & II* would not change any of the conclusions reached so far, since the current tests successfully managed to capture the peak lift coefficient for both  $C_L$  surfaces created. The main objective of conducting the *free-response* VIV experiments with two different sets of springs was to observe the maximum lift coefficient at two separate supercritical Reynolds numbers and thus investigate whether the Reynolds number influences the hydrodynamic coefficients of vibrating cylinders in a manner similar to what has been observed in subcritical Reynolds number tests. Comparison of the  $C_L$  surfaces presented in Figs. 9 and 11 reveal that around the peak of the surface, the  $C_L$  values for the lower of the two supercritical Reynolds ranges tends to be consistently larger by a small amount than the values computed for the higher supercritical Reynolds number range, typically between 5% to 15% larger. The comparison of the peak lift coefficients, corresponding to each one of the supercritical Reynolds number ranges, is further discussed in Section 5. The differences in the computed  $C_M$  surfaces are very small and are typically within  $\pm 5\%$  in the vicinity of the  $A/D$  vs.  $V_{Rn}$  regions leading to peak response conditions. The preliminary conclusion is that after one takes into consideration both the experimental uncertainties and the inherent VIV response variability that exist in these tests, the computed lift coefficient and added mass coefficient values are quite similar in magnitude for both supercritical Reynolds numbers and hence show only a weak Reynolds number dependence over the range tested.

#### 4.3. Hydrodynamic coefficients from free-response VIV data (December tests)

The opportunity arose to conduct a second round of testing in December 2015. Applying the lessons learned from the first round of tests, a one-day test program was conducted with the emphasis placed on more *free-response* VIV tests with a greater range of damping values, so as to create more complete  $C_L$  and  $C_M$  surfaces. In the March tests it was concluded that testing at the higher Reynolds number resulted in very large dynamic forces which increased the risk of damaging the towing carriage and test setup. Therefore, the decision was made to test only with the softer of the two spring settings and hence at the lower of the two supercritical Reynolds number ranges. All of the December 2015, *free-response* VIV tests were conducted with the softer set of springs at 23.58 kN/m with the peak response occurring at  $5 < V_{Rn} < 6.6$  corresponding to a Reynolds number of  $3.3 \times 10^5 < Re < 4.3 \times 10^5$ .

By using more and different combinations of resistors connected across the damping servo-motor's terminals the cylinder's response was tested at damping ratios of  $\zeta \sim 0.49, 0.23, 0.20, 0.16, 0.10$ . Two further damping ratio values of  $\sim 0.03$  and  $\sim 0$  were achieved by using the damping compensation motor in its original intended form, where it was used to inject some energy back into the system to counteract the energy dissipated in all the mechanical linkages (corresponding to the  $\zeta \sim 0.10$  case). Fig. 12 shows the cross-flow response amplitudes as a function of the different amounts of damping present in the system. The largest response amplitudes recorded for  $\zeta \sim 0.03$  and  $\zeta \sim 0$  were very close to 0.88D which is similar to the largest response amplitudes ever recorded at this facility in the pure cross-flow motion configuration. The limit-cycle amplitude for this cylinder and spring setup lies very close to the orange colored curve corresponding  $\zeta \sim 0$  in Fig. 12 and it is interesting to note that the  $\zeta \sim 0.03$  has a peak response amplitude very close to the nearly  $\zeta \sim 0$  damping case with the only substantial difference lying in the region  $4 < V_{Rn} < 5$ . The proximity of these two curves also indicates that the  $C_L$  surface will be very steep in this vicinity.

These additional runs, with lower damping values than what had been previously achieved in the March 2015 tests, allowed the computation of lift and added mass coefficients in what was labeled as *Region II* during the discussion of Fig. 11. Similarly, runs with higher damping values than had been previously achieved during the first round of testing, allowed finding coefficients for the region labeled as *Region I* in Fig. 11. The testing window during this second round of testing allowed for approximately 10–12 ramp tests and therefore there was not enough time available to execute multiple repeats for each damping setting which is the reason that some of the curves in Fig. 12 are unlike the smoother curves shown in Fig. 8 and Fig. 10 which benefitted from more averaging over multiple repeated ramp tests. Clearly the response data collected, especially at the higher damping levels, would have benefitted greatly from repeated ramp tests to better characterize the response variability and obtain more meaningful statistics.

Only increasing speed ramp tests were conducted during the December testing window. The results from the ramp tests are presented in a similar manner to Figs. 8 and 10 earlier. For the damping values of  $\zeta \sim 0, 0.03, 0.10, 0.20$  the curves represent the mean values of the ramp extracted results at each reduced velocity value and the shaded region represents  $\pm 1$  st. dev. around the mean. For damping values of  $\zeta \sim 0.16, 0.23, 0.49$  only a single ramp test was conducted for each damping setting value and hence it is not possible to compute a standard deviation. The figures also include the values measured during four steady towing speed tests for the  $\zeta \sim 0.10$  damping setting. Two of these steady towing speed tests were conducted at  $V_{Rn} \sim 5.4$  and resulted in similar responses.



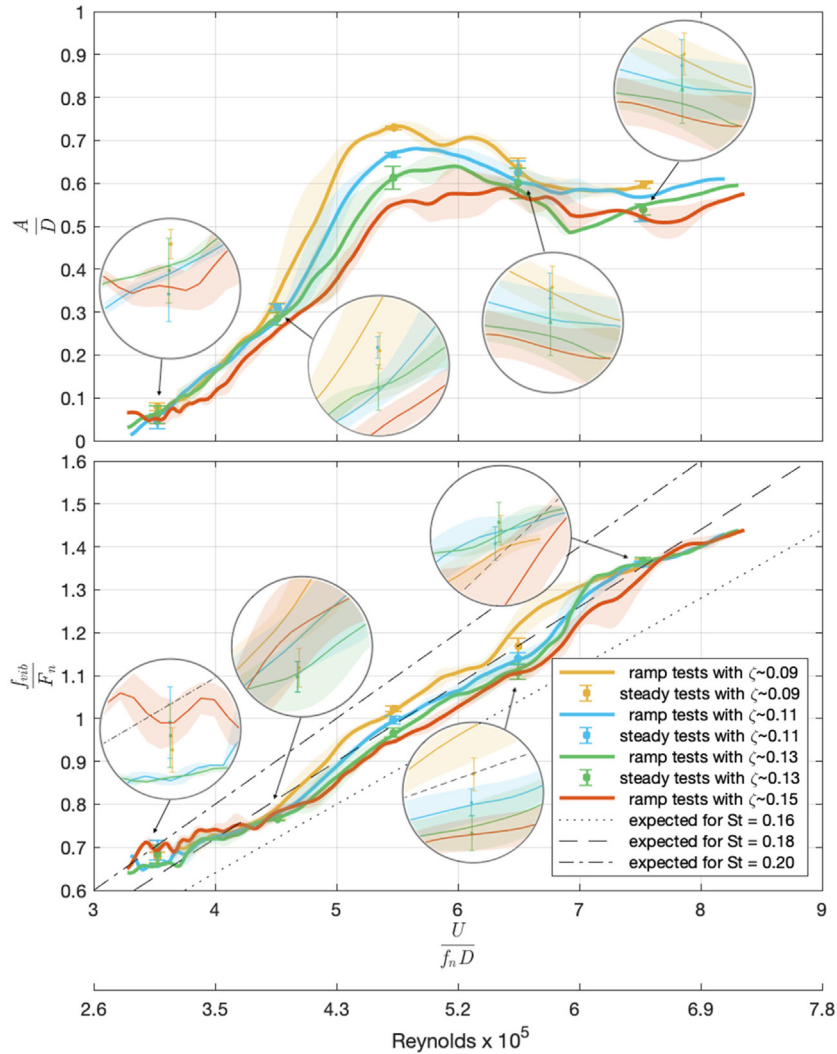


**Fig. 8.** Dimensionless response amplitude (TOP) & dim. resp. frequency (BOTTOM) vs. reduced velocity or Reynolds number for four different damping settings in the March tests with the stiff springs ( $f_n \sim 0.90$  Hz). (For interpretation of the references to color in this figure legend, the reader is referred to the web version of this article.)

Fig. 13 shows the contours of lift and added mass coefficients, respectively, as a function of the nominal reduced velocity and dimensionless response amplitude. These figures represent the most complete contours of lift and added mass coefficient that are computable from *free-response* VIV tests without having to resort to using external perturbations. Obtaining a little more data to further populate the contours at very small  $A/D$  values might be possible by increasing damping even more than what was presently achieved but the additional data is not expected to change the shape of the contours significantly given the very mild slopes of the coefficient surfaces in those regions. Finally, it should be reiterated that populating the contours at  $A/D$  values higher than  $0.9D$  and for reduced velocities smaller than 4 is not possible without resorting to *forced-vibration* or providing the cylinder with an external perturbation in the form of an initial condition. This boundary represents the limit-cycle boundary beyond which *self-excited* vibration is not possible. Because the surface does not extend to negative  $C_L$  values, the exact location of the  $C_L = 0$  contour cannot be drawn. This would closely follow the  $A/D$  vs.  $V_{Rn}$  curve for the  $\zeta \sim 0$  ramp tests. The maximum lift coefficient computed for this surface is 0.81 and occurs at  $A/D = 0.65$  and  $V_{Rn} = 5.9$  which is very close to the value of 0.84 occurring at  $A/D = 0.62$  and  $V_{Rn} = 5.9$  computed from the *free-response* test using the same soft springs in the March tests and shows the repeatability between the two rounds of testing. In the central portion of the surfaces shown for each of the two rounds of testing, both the  $C_L$  and  $C_M$  coefficients typically agree within  $\pm 5\%$  which is well within the typical uncertainties associated with computing these coefficients. The experimental uncertainty is due to the inherent variability that exists in the response data and the limitations that exist when quantifying the system damping present. These issues are presented in further detail in the following section.

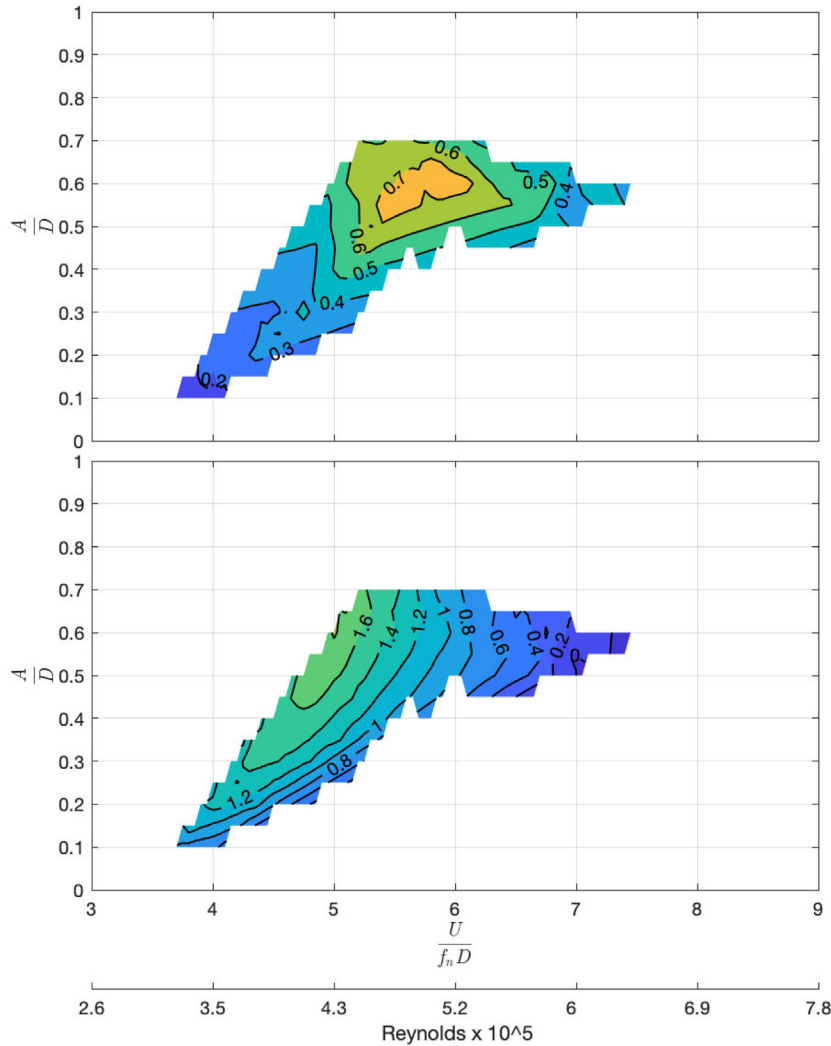


**Fig. 9.**  $C_L$  contours (TOP) and  $C_M$  contours (BOTTOM) from the March tests with the stiff springs ( $f_n \sim 0.90$  Hz). (For interpretation of the references to color in this figure legend, the reader is referred to the web version of this article.)

#### 4.4. Comparisons between the march and december tests and other relevant datasets

Fig. 14 shows the peak response amplitude as a function of the dimensionless damping present in the system. The peak amplitude is the largest amplitude measured for each spring-damping setting and does not need to occur at the same reduced velocity value. In fact, the data presented earlier shows that increasing the damping tends to shift the peak response amplitude to slightly higher values of reduced velocity. The figure includes error-bars, drawn at  $\pm 1$  st. dev. for the peak response amplitude, to reflect the inherent response variability that exists in the response data. When a particular test was not repeated enough times to gather meaningful statistics no vertical error-bars are shown. The figure also includes error bars drawn at  $\pm 1$  st. dev. to reflect the uncertainties that exist in the measurement of the dimensionless damping. These stem from both the uncertainty that exists in quantifying the system damping as well as the variability that exists in the response frequency. One of the reasons for including this plot is to demonstrate the good agreement and repeatability between the first and second round of testing after the experimental uncertainties are taken into consideration. The results for the softer springs that correspond to the lower Reynolds number range show very good agreement between the two rounds of testing conducted in March and December. The other reason to show the peak VIV response amplitude as a function of the dimensionless damping is to facilitate the identification of Reynolds number effects. Upon first inspection, the data collected in this investigation shows similar response amplitudes at the same values of dimensionless damping after taking into consideration the experimental uncertainties and the inherent response variability that can exist in high Reynolds number data. Closer inspection reveals that the response amplitude

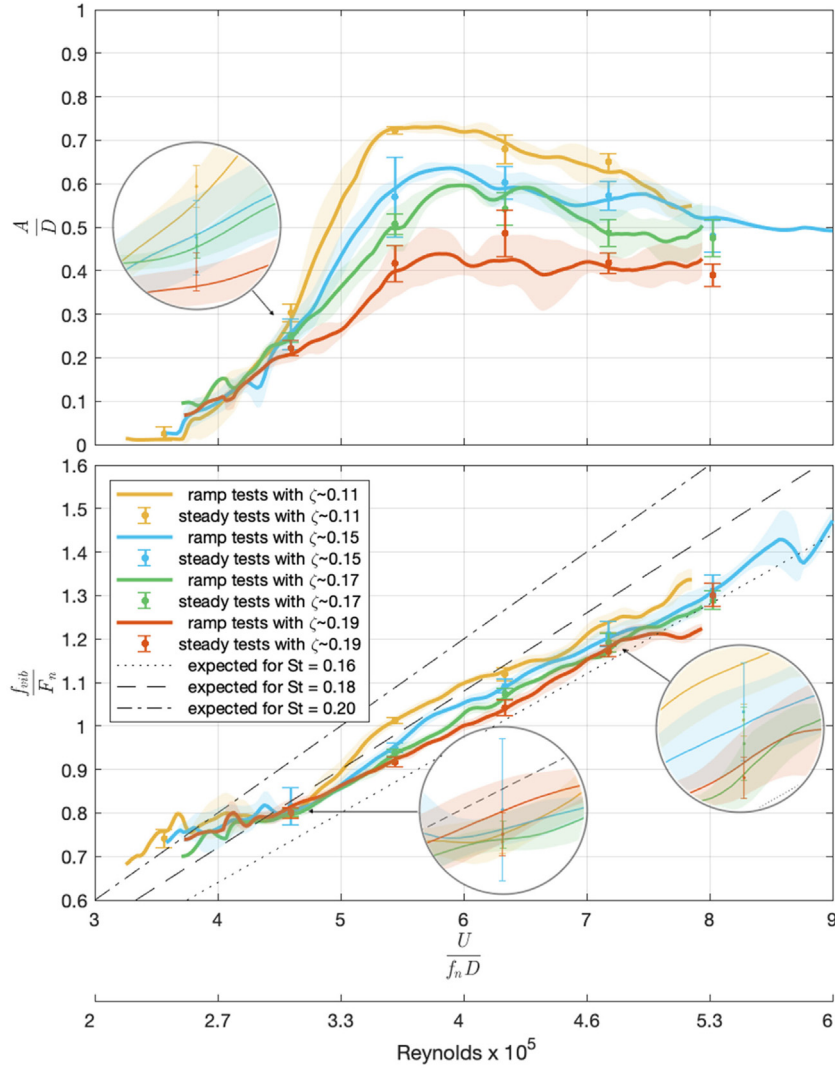


**Fig. 10.** Dimensionless response amplitude (TOP) & dim. resp. frequency (BOTTOM) vs. reduced velocity or Reynolds number for four different damping settings in the March tests with the soft springs ( $f_n \sim 0.69$  Hz). (For interpretation of the references to color in this figure legend, the reader is referred to the web version of this article.)

data for the higher of the two supercritical Reynolds number ranges is consistently smaller than or at most equal to the peak response amplitude at the lower of the two supercritical Reynolds numbers when these are compared at similar values of dimensionless damping. On an  $A^*$  vs.  $c^*$  plot like Fig. 14, the lines of constant lift coefficient appear as hyperbolas due to  $C_L = c^*A^*$  relationship. The smaller lift coefficients appear towards the bottom left-hand side and the hyperbolas corresponding to larger lift coefficient values appear towards the upper right-hand side. Comparing the measured response amplitude at a given value of dimensionless damping  $c^*$  is directly equivalent to comparing the lift coefficient values.

Fig. 15 shows the same information included in Fig. 14 but cast in the guise of lift coefficient curves that result from the computing  $C_L$  values using the  $C_L = c^*A^*$  relationships for each data-point that was shown in Fig. 14. These lift coefficient curves that show the dependance of  $C_L$  on the response amplitude,  $A/D$ , are equivalent to taking a (slightly diagonal) ‘slice’ through each of the 2-dimensional surfaces shown earlier in Fig. 9, Fig. 11 and Fig. 13. When the peak response data corresponding to different amounts of system damping is compared in this form, again it is evident that results from the second round of tests agrees well with the first round of testing after experimental uncertainties are taken into account. It is also evident that even though the maximum lift coefficients are similar for the lower and the higher Reynolds number ranges, the latter shows consistently smaller lift coefficient values. Similar conclusions can be reached after carefully examining and comparing the 2-dimensional surfaces shown earlier. It is important to note that the uncertainties shown in the computed lift coefficient value are not negligible and after taking these into consideration it is much harder to decisively conclude whether Reynolds effects exist in the supercritical region tested in this investigation

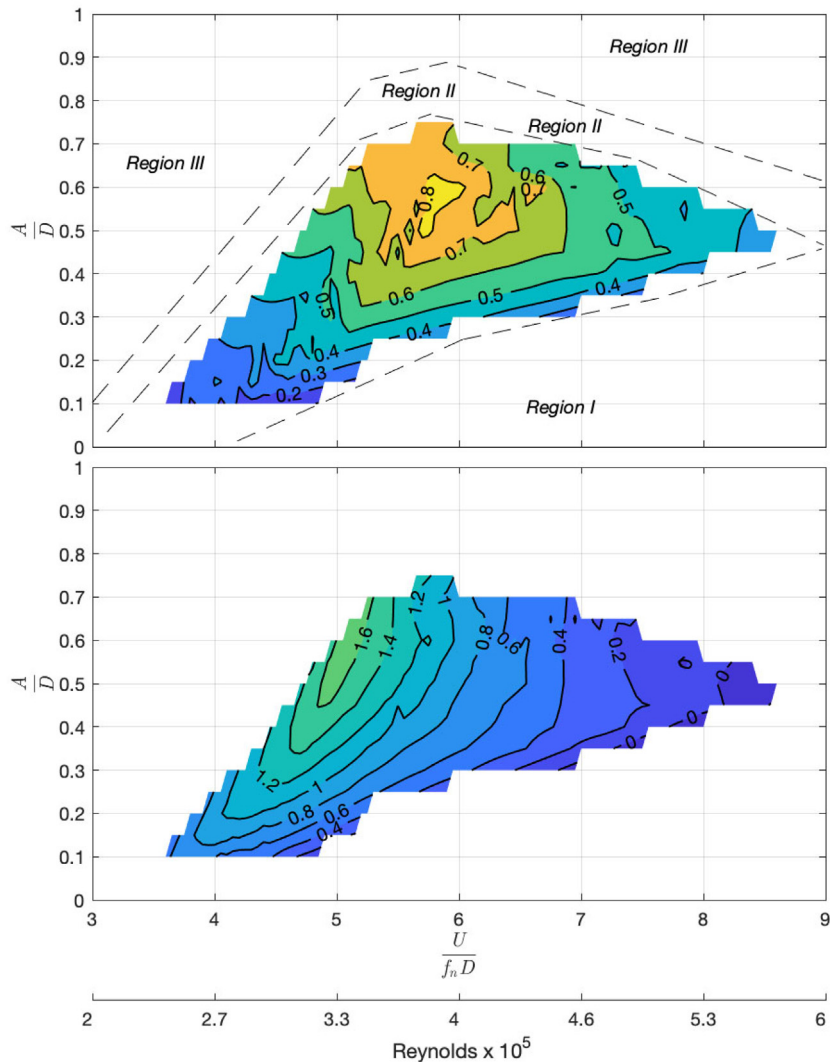


**Fig. 11.**  $C_L$  contours (TOP) and  $C_M$  contours (BOTTOM) from the March tests with the soft springs ( $f_n \sim 0.69$  Hz). (For interpretation of the references to color in this figure legend, the reader is referred to the web version of this article.)

or whether these results are due to experimental uncertainties and inherent response variability. The weak supercritical Reynolds number effects identified in this investigation support the conclusion of Yin et al. (2017, 2018). It appears that for a given surface roughness, the Reynolds number effects in the supercritical region are weaker than those known to exist in the subcritical regime.

In the subcritical regime, the Reynolds effects result in the response amplitude increasing as the Reynolds number is increased. The exact value of the limit-cycle response amplitude and the maximum lift coefficients also depend on particular details like aspect ratio, surface roughness, end effects, etc. which greatly complicates direct comparisons between different datasets but the general Reynolds effect within a particular dataset set is always consistent in the subcritical regime. Specifically, a relatively small change in Reynolds number is sufficient to lead to obvious Reynolds number effects if the dimensionless damping is properly accounted for. This effect is easier seen when substantial amounts of damping are present and the maximum lift coefficients at the different Reynolds numbers can be directly compared. Resvanis et al. (2012) demonstrate this for data from Govardhan and Williamson (2006) and Klamt et al. (2005). For the former dataset the maximum lift coefficient is found to increase from  $C_L \sim 0.28$  to  $C_L \sim 0.38$  when the Reynolds number increases from  $\sim 1000$  to  $\sim 12,000$ . For the later dataset, the maximum lift coefficient is found to increase from  $C_L \sim 0.37 - 0.40$  at a  $Re \sim 500$  to approximately  $C_L \sim 0.65$  by the time the Reynolds number is increased to 2400. Similar behavior is shown in Vandiver (2012) using the data of Lee and Bernitsas (2011) where it is demonstrated that the maximum lift coefficient increases from  $C_L \sim 0.65$  at  $Re \sim 47,000$  to a value of  $C_L \sim 0.95$  at  $Re \sim 86,000$ . For small amounts or virtually zero damping, the Reynolds number effects in the subcritical region are best illustrated by

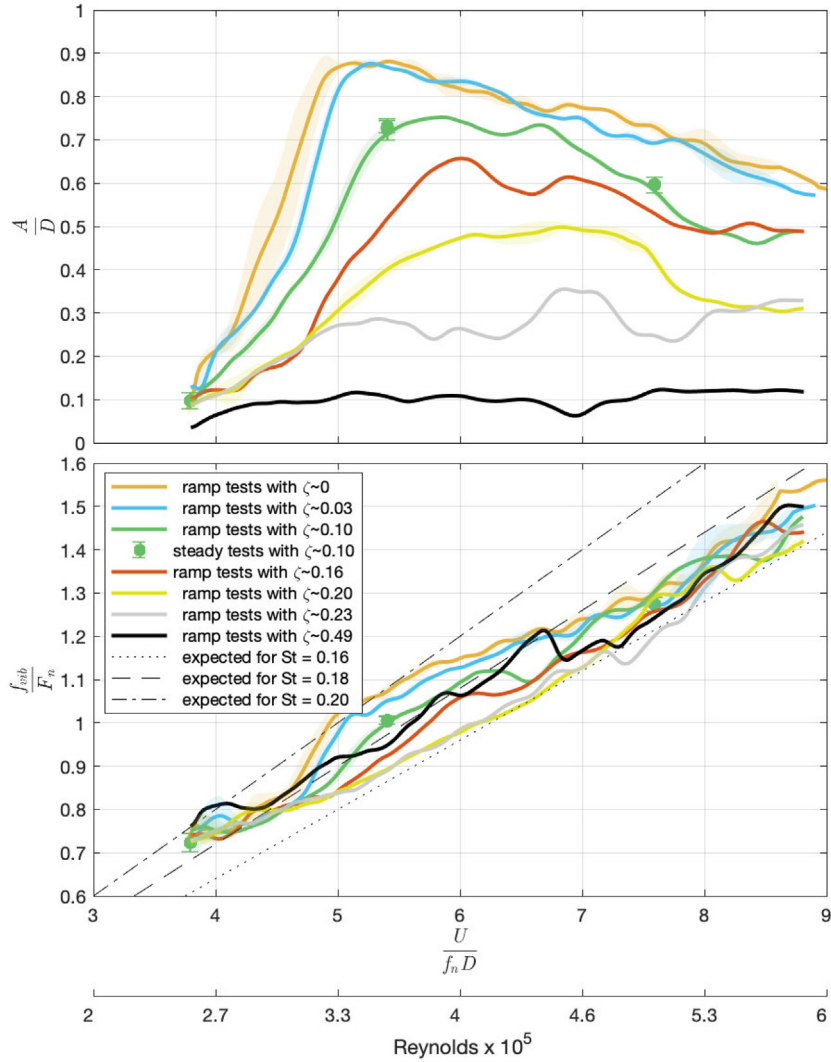


**Fig. 12.** Dimensionless response amplitude (TOP) & dim. resp. frequency (BOTTOM) vs. reduced velocity or Reynolds number for seven different damping settings in the December tests with the soft springs ( $f_n \sim 0.69$  Hz). (For interpretation of the references to color in this figure legend, the reader is referred to the web version of this article.)

comparing the changes in the limit-cycle amplitude (*i.e.* the VIV response amplitude corresponding to  $C_L \sim 0$ ). The data collected by Blevins and Coughran (2009) clearly shows the maximum response amplitude changing from  $A/D \sim 0.65$  at  $Re \sim 10^3$  to more than double that value and reaching  $A/D \sim 1.5$  at  $Re \sim 10^5$  for their test cylinder when they kept the system damping very low.

In contrast, the  $\sim 10^5$  difference in Reynolds numbers in the peak response (or max  $C_L$ ) observed for the two different spring stiffness setups that were used in this investigation, is simply not a sufficiently large variation of Reynolds number in the supercritical regime to be able to draw firm conclusions regarding these weak effects. More tests with different combinations of springs that would result in peak response occurring at lower and even higher Reynolds numbers would be necessary in order to confirm whether the slight decrease in  $C_L$  that was observed in this investigation, is in fact a real trend in the data or just a result of experimental uncertainties and the stochastic nature of VIV.

The response amplitude information presented at supercritical Reynolds numbers by Dahl et al. (2010) is not directly comparable because even though they used the exact same cylinder model they had also allowed in-line motion in their tests. Any comparison between the *free-response* cross-flow response amplitudes that they reported and the results shown in this work is only meaningful so as to illustrate the effects that can occur after allowing a cylinder to also vibrate in the in-line direction. In their work they report a cross-flow amplitude as large as  $0.8D$ . Their peak value occurs at a higher reduced velocity of  $V_{Rvib} \sim 6.6$  which is entirely consistent with what is known regarding combined cross-flow and in-line *free-response* VIV testing at smaller laboratory scales.



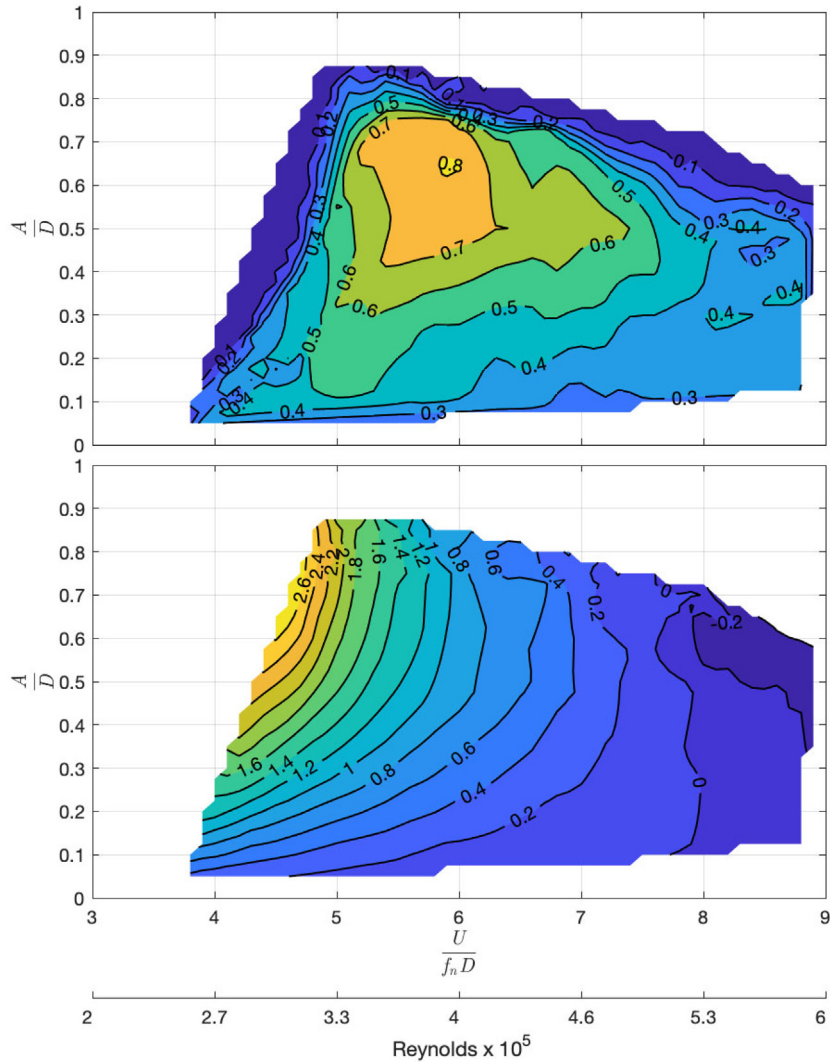


**Fig. 13.**  $C_L$  contours (TOP) and  $C_M$  contours (BOTTOM) from the December tests with the soft springs ( $f_n \sim 0.69$  Hz). (For interpretation of the references to color in this figure legend, the reader is referred to the web version of this article.)

The *free-response* amplitude data reported by Lie et al. (2013) is not directly comparable with this investigation due to the different surface roughness, the substantially different aspect-ratio ( $L/D \sim 6$ ) and the test cylinder's orientation which pierced the free surface. During their follow up testing at the same facility using a surface piercing cylinder with,  $L/D \sim 6$  and  $k_s/D \sim 1 \times 10^{-3}$ , albeit at slightly different Reynolds number, the authors reported pure cross-flow *free-response* peak response amplitudes of  $0.65D$  and the lift coefficient values measured using *forced-vibration* tests on the same cylinder were slightly greater than  $0.3$  (Yin et al., 2017, 2018). The authors do state that they might have seen larger amplitudes if more tests were conducted and values were not interpolated in the region of the lift coefficient surface where the maximum value was observed. The main causes for the differences observed between their results and the results described in this investigation, is the short aspect ratio and the surface roughness which might not be sufficiently rough to ensure that their tests conducted at  $Re \sim 4 \times 10^5$  are outside the drag-crisis region. At the time of writing this manuscript, SINTEF Ocean (formerly MARINTEK) has completed fabrication of a new large-scale high Reynolds number VIV test rig (Yin et al., 2020). This new test rig will allow for much larger aspect ratios than their original riser model and will be orientated horizontally but no results have been published so far.

The most closely comparable *free-response* VIV data is the limited data shown in Ding et al. (2004). Unfortunately, the authors do not report the exact Reynolds numbers for their test case using the large surface roughness model which would be directly comparable to the cylinder used in this investigation. During their investigation, they carefully traced out the drag-crisis region for the various cylinders used, so one expects that they avoided running their test in the Reynolds region that would cause the most problems but exact values are not provided for the test data that is most comparable to this

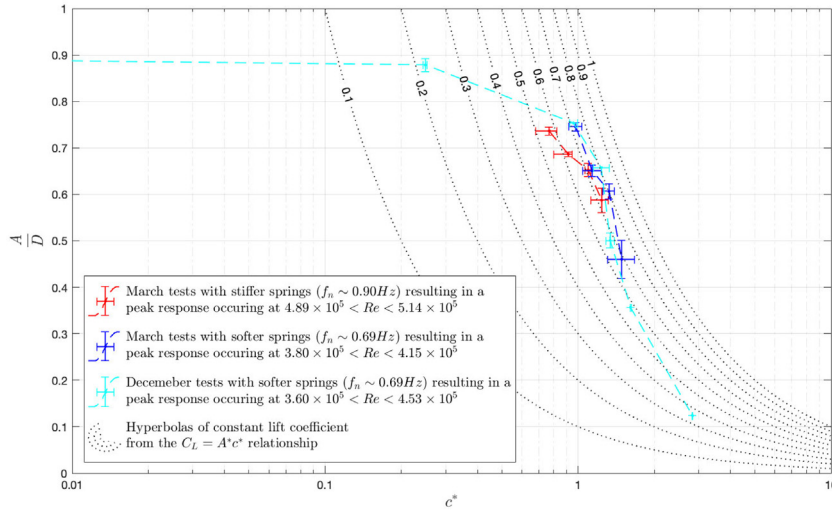


**Fig. 14.** Peak dimensionless response amplitude vs dimensionless damping. (For interpretation of the references to color in this figure legend, the reader is referred to the web version of this article.)

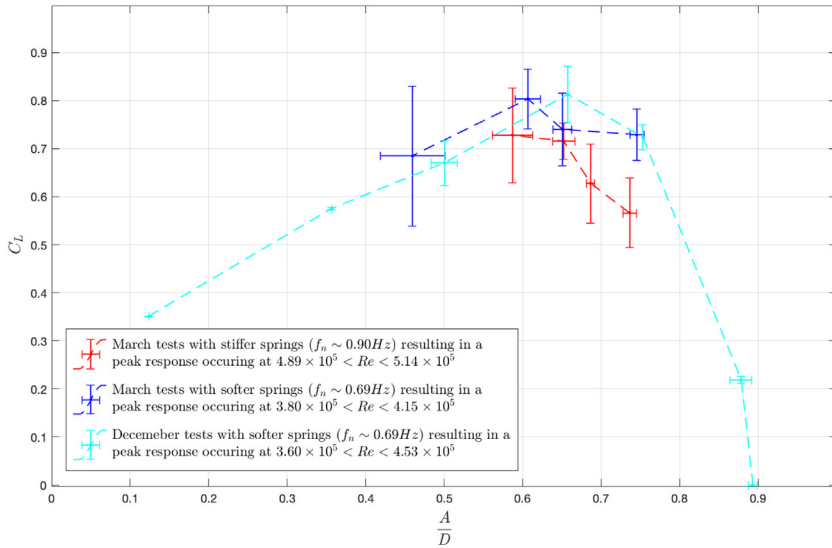


**Fig. 15.** Lift coefficient vs. response amplitude for the two supercritical Reynolds number ranges tested. (For interpretation of the references to color in this figure legend, the reader is referred to the web version of this article.)

investigation. They report a maximum response amplitude of 0.85D to 0.9D which is very similar to the maximum value of 0.89D reported in this investigation (see Figure 7 in (Ding et al., 2004)). The shape of the lift coefficient surface that they computed (see Figure 11 in (Ding et al., 2004)) is also very similar to what was computed here, the main difference being that the largest lift coefficient contour that they report is 0.5 whereas the largest lift coefficient reported in this investigation is  $C_L \sim 0.8$ . Further comparisons with their reported lift coefficient values will not be made because they do not report the exact Reynolds number for the data used for in that figure. Additionally, in light of their comment regarding “interpolation between actual data points was required to generate the contours”, it is not clear if a sufficient number of runs was included in their test matrix to thoroughly explore the lift coefficient values where the maximum occurred. They conducted discrete steady speed tests, with just 8 tests covering the region between  $3 < V_{Rn} < 9$  at a given damping setting. In our investigation the variation of response amplitude (and equivalently the  $C_L$  or  $C_M$  surfaces) with reduced velocity is fully covered due to the continuous ramp tests. Interpolation is only used to populate lift or added

mass coefficient surfaces across the  $A/D$  dimension and even then, it is limited since a sufficient number of damping values was chosen to fully investigate the response amplitude's dependence on damping.

In this investigation, most runs were repeated numerous times and the maximum lift coefficient from all three test configurations (two spring stiffnesses in the March tests and one spring stiffness repeated in the December tests) was consistently in the neighborhood of  $C_L \sim 0.8$  when calculated using Eq. (5). As discussed earlier, apart from the inherent response variability another large source of uncertainty in this investigation was the quantification of the amount of damping present in the system. In addition to the damping that was added to the system by modifying the servo-motor into a generator, the VIV testing apparatus has multiple sources of additional damping in the various mechanical linkages and connections and we did not have the ability to carefully and fully characterize this behavior (amplitude dependence, frequency dependence, etc.).

For a few select test runs where the largest lift coefficients were observed, the coefficients computed using Eqs. (4) & (5) were compared directly with the coefficients computed from the measured load cells on the internal dynamometer. For example, during a particular ramp test where large lift coefficient values were observed, when the peak lift coefficient computed from Eq. (5) was 0.74 (at  $V_{Rn} \sim 6.08$ ), the lift coefficient from the directly measured lift forces was 0.69 (at  $V_{Rn} \sim 6.06$ ). Similarly, the added mass coefficient computed using Eq. (4) had a maximum value of 1.07 (at  $V_{Rn} \sim 5.4$ ) compared to a value of 1.05 (at  $V_{Rn} \sim 5.38$ ) when calculated directly from the lift forces in phase with the cylinder acceleration. The comparisons at other reduced velocity values show that the added mass and lift surfaces shown previously have the correct shapes. Our observations from several such comparisons between the load cell calculated values and the quantities computed using Eqs. (4) & (5) shows good agreement for the added mass coefficient but there is a tendency for the Eq. (5) computed lift coefficient to overestimate the load cell measured values by up to 10%–20% for some of the tests with lower damping that result in very high response amplitudes but small lift coefficients. This is attributed to an over-estimation of the amount of damping present in the system and subsequently used in Eq. (5) and is the greatest source of uncertainty in these computations. These smaller lift coefficients that correspond to largest response amplitudes are not as critical to our investigation which aimed to identify Reynolds number effects on the maximum lift coefficient.

The maximum lift coefficient measured during the DeepStar *forced-vibration* experiments (DeepStar, 2003) using the same testing facility 15 years earlier was 0.82 at  $A/D = 0.5$  and  $V_{Rvib} = 6$  which compares nicely with the maximum  $C_L$  value of 0.83 occurring at  $A/D = 0.5$  and  $V_{Rvib} = 5.9$  obtained from the *free-response* tests in this investigation after all the available increasing ramp data (from both Reynolds number ranges and both rounds of testing) is collated and the force coefficient surfaces are plotted against the true reduced velocity instead of the nominal reduced velocity. The comparison between the key elements of the lift coefficient surfaces that were measured in the DeepStar *forced-vibration* tests and those computed from the *free-response* data in this investigation is shown in Appendix B.

Complete added mass coefficient data from *free-response* VIV tests is not publicly available at these large Reynolds values. Unlike the lift coefficient data from the DeepStar *forced-vibration* data presented above, the added mass coefficient data in the data repository (DeepStar, 2003) is believed to contain a transcription error. Close inspection of the tabulated data reveals that it does not agree with the accompanying figure in the repository and therefore comparisons with the added mass coefficients computed in these *free-response* tests cannot be made. As discussed earlier, the added mass coefficients computed from Eq. (4) were always in good agreement when compared to the measured dynamometer loads that are in phase with the cylinder acceleration during the same *free-response* tests. The added mass contours computed and presented herein show the expected shape and behavior that is known from low Reynolds and subcritical Reynolds tests. At reduced velocities smaller than the critical reduced velocity the added mass coefficient is larger than the still-water value and at reduced velocities larger than the critical reduced velocity the added mass coefficient decreases to values smaller than the still-water added mass. This gradual variation in added mass is necessary in order to change the oscillator's effective natural frequency and allow it to synchronize with the shed vortices.

## 5. Conclusions

To date, there have only been a handful of attempts to collect the data necessary to populate the hydrodynamic databases necessary for predicting VIV at supercritical Reynolds numbers. The limited data that does exist remains the proprietary information of the organizations that funded those investigations. The primary objective of this work was to explore a new way of performing prototype scale model tests in order to extract the necessary hydrodynamic coefficients and to obtain VIV response data at very high Reynolds numbers in a more efficient manner. The main focus was on demonstrating that *free-response* VIV tests with variable amounts of damping are suitable for calculating the desired lift coefficient,  $C_L$ , and added mass coefficient,  $C_M$ , based purely on the measured response amplitude, response frequency and the governing equations. Additionally, it was demonstrated that a small number of carefully planned variable towing speed tests (*i.e.* ramp tests) can provide the same VIV response data as that which would otherwise have required dozens or hundreds of constant speed tests.

The experimental results confirmed that the two approaches to model testing described here yielded satisfactory results and allowed the extraction of the hydrodynamic coefficients of interest, namely the lift coefficient and added mass coefficients as a function of response amplitude and reduced velocity. Specifically, Vandiver's (2012) proposed approach to calculating lift coefficients solely based on the response amplitude and frequency and knowledge of the dimensionless damping present in the system is shown to be an effective way of obtaining the necessary hydrodynamic data. Because this type of testing relies on *free-response* VIV tests one does not have to deal with the more complicated *forced-vibration* equipment and the large test matrices that result from all the possible combinations of externally prescribed amplitude, forcing frequency and flow velocity *etc.*

The carefully executed ramp tests and the comparison with the results from traditional steady speed tests demonstrated that carefully planned variable speed tests can cover a much broader matrix of test conditions than would have been possible with a small number of conventional constant speed tests and in considerably less time. At a suitably long facility just one carefully planned ramp test, running through the tank at continuously varying speeds, will yield all the information necessary to characterize the VIV response as function of the reduced velocity. The variable-speed towing tests or 'ramp tests' results into considerably fewer runs necessary to fully characterize the VIV behavior for the desired range of conditions and allows the investigator to spend his 'tank time' in a more useful and constructive manner. If desired, additional ramp tests can be repeated and the information can then be used to characterize the inherent response variability that exists at high Reynolds numbers. Both the steady test results as well as the variable speed results show considerable response variability at certain values of reduced velocity and there is a need to understand what mechanisms are responsible for this observed behavior in the supercritical Reynolds regime

In the follow-up testing performed in December of 2015, it was successfully demonstrated that a handful of runs through the towing tank at variable speeds, each with various amounts of damping, is sufficient to extract the complete surfaces of added mass and lift coefficient data where self-excited VIV is possible. The desired hydrodynamic data can be fully computed from the measured response quantities without needing to resort to *forced-vibration* testing with a test matrix that would easily have been two orders of magnitude larger.

The Reynolds number effects observed in the supercritical Reynolds range investigated in this paper are weak. Given the response variability that was observed in the supercritical Reynolds data in both the cylinder's response amplitude and frequency and the uncertainties that exist in the damping quantification, it is not possible to conclude the definitive existence of a weak Reynolds effect on the lift coefficient in the supercritical region. One would need to conduct tests at even higher Reynolds numbers and with more intermediate points before confirming whether a definite trend with the Reynolds number exists in the supercritical data or the slight difference in the values observed in this investigation is the result of the weakly stochastic nature of VIV. Since the coefficient surfaces computed and shown here for both Reynolds numbers ranges tested are so similar in magnitude and shape, the data could easily be combined into a single database.

The experimental evidence strongly suggests that in these slowly varying flows the cylinder has adequate time to respond to the slowly changing flow conditions and slowly varying hydrodynamic forces. The largest differences between steady test results and varying speed results and more specifically the response in accelerating or decelerating flow are typically limited to regions with strong hysteretic effects. In these regions the prior flow history has already set the cylinder response at a specific frequency with little impetus to vary. The primary focus of studying the VIV response in slowly-time varying flows in this investigation was to show that they are suitable alternatives to many individual steady speed tests.

Additionally, the comparisons between the steady and slowly-time varying flow results can also inform our approach to the VIV response prediction of long slender cylindrical structures exposed to slowly changing ocean currents. Future work on VIV in time-varying flows needs to investigate the relationship between maximum permissible  $\gamma$  values that will still result in response amplitudes as large as those seen in steady tests and how these maximum permissible values of  $\gamma$  vary with system damping and cylinder mass-ratio.

## Nomenclature

$Re$	Reynolds number
$St$	Strouhal number
$C_y$	Total excitation coefficient
$C_L$	Lift coefficient
$C_M$	Added mass coefficient
$C_D$	Drag coefficient
$V_{Rn}$	Nominal reduced velocity (based on the still-water natural frequency, $f_n$ )
$V_{Rvib}$	True reduced velocity (based on the actual response frequency, $f_{vib}$ )
$f_n$	Still-water natural frequency (Hz)
$T_n$	Still-water natural period (s)
$k$	Total stiffness for the springs supporting the rigid cylinder
$k_{eff}^*$	Dimensionless effective stiffness
$k_s$	Surface roughness
$m$	Total oscillating mass of rigid cylinder, including any trapped water and attached linkages and mechanical components but without the external fluid “added mass”
$c$	Damping coefficient
$c^*$	dimensionless damping coefficient
$D$	Hydrodynamic diameter of cylinder (including the roughness jacket)
$L$	Cylinder's length
$L_{dyno}$	Portion of the cylinder's length that acts on the internal dynamometer
$F_{CF}$	Total cross-flow force
$F_{IL}$	Total in-line force
$k_s$	Surface roughness
$y(t)$	The cylinder's time varying response (displacement) in the cross-flow direction
$\dot{y}(t)$	The cylinder's response velocity in the cross-flow direction
$\ddot{y}(t)$	The cylinder's response acceleration in the cross-flow direction
$Y_{RMS}$	The RMS value of the cylinder's displacement
$A$	The cylinder's response amplitude
$A^*$	The dimensionless response amplitude
$T_{vib}$	Response period (s)
$F_{shed}$	Vortex shedding frequency (Hz)
$T_{shed}$	Vortex shedding period (s)
$f_n$	Still-water natural frequency (Hz)
$f_{vib}$	The cylinder's response frequency (Hz)
$t$	Time (s)
$U$	Towing velocity (m/s)
$\zeta$	Damping ratio (fraction of critical damping)
$\omega_d$	Damped still-water natural frequency (rad/s)
$\omega$	Excitation and response frequency (rad/s)
$\omega_n$	Still-water natural frequency (rad/s)
$\gamma$	Gamma parameter
$\rho$	Density of water
$\nu$	Kinematic viscosity of water
$\varphi$	Phase difference between the cylinder's response and the fluid forcing
$\Omega$	Electrical resistance ( $\Omega$ )

## Declaration of competing interest

The authors declare that they have no known competing financial interests or personal relationships that could have appeared to influence the work reported in this paper.

## Acknowledgments

The authors would like to acknowledge Lockheed Martin Corporation and Statoil for funding the first round of these tests and the SHEAR7 Joint Industry Project members for their support and funding during the second round of tests and MIT SHEAR7 Joint Industry Project, Cambridge, MA, USA. The authors are indebted to Royal Dutch Shell and AMOG Consulting & Matrix Composites for their collaboration and their willingness to cover the mobilization costs for installing the VIV testing rig in the NRC towing tank during each round of testing respectively. Special thanks are due to the



anonymous reviewers for their careful review of this manuscript and their extremely useful feedback and comments. Finally, these tests would not have been possible without the ingenuity of Don Spencer who designed the original test rig for the DeepStar, Joint Industry Project, Panel 5402 and the hard work of the multiple engineers, riggers and divers from Oceanic Consulting Corp. and the NRC towing tank at St. Johns, Newfoundland.

## Appendix A. Drag coefficients for fixed and freely vibrating cylinders

Experiments were performed at both steady and constantly varying towing speeds with the cylinder both fixed and free to respond to the external flow. The goal of the *fixed cylinder drag tests* was to measure the drag loads and to calculate drag coefficients for fixed (*i.e.* stationary) cylinders over a large range of Reynolds numbers. The very small variation in the measured drag coefficient that was observed from  $2 \times 10^5 < Re < 1 \times 10^6$  combined with the large variation that was observed when the Reynolds number was lower ( $Re < 1 \times 10^5$ ) supports the claim that the free-response VIV tests which are the main focus of this investigation were being conducted in what is the supercritical Reynolds regime for this cylinder and surface roughness. These observations are complemented by past experience testing very smooth surfaced cylinders at the same facility. At the same Reynolds numbers that the rough surface cylinder used in this investigation systematically experienced self-excited oscillations due to VIV as large as 0.8–0.9D, the smooth surfaced cylinder barely vibrated at 0.05D (DeepStar, 2003). In the DeepStar tests when the smooth surfaced cylinder was tested it was necessary to install a turbulence screen before noteworthy VIV were observed. This kind of behavior is indicative of the response in the critical Reynolds regime. Because the motivation is to study cylinder VIV, a roughness jacket has been used for most subsequent VIV investigations at this facility.

The drag loads on the cylinder were continuously recorded by the dynamometer load cells in the in-line direction (*i.e.* towing direction) during both the *fixed cylinder drag tests* and the *free-response* VIV tests. The drag coefficient from a variable speed test (ramp test) can be calculated in the usual manner but as previously discussed all statistical quantities of interest need to be computed using a moving or running window that will pass through the entire time-series. All averaging was done using a moving-window that was 5 cycles long. Because in this arrangement the cylinder is fixed and there is no natural period for the system, the moving-window length that was used corresponded to approximately 5 vortex-shedding periods, with the shedding period being estimated from the Strouhal relationship. The estimated vortex shedding period is also used as the relevant time-scale for the numerator of the  $\gamma$  parameter listed in Eq. (6). The constantly varying ramp tests when the cylinder was in the fixed arrangement attempted to keep  $\gamma < 0.02$  in a similar manner to ramp tests for the *free-response* tests.

In Eq. (11),  $\bar{F}_{IL}(t)$  is the mean drag force recorded by the dynamometer and  $\bar{U}(t)$  is the mean towing speed computed from within these moving windows.

$$C_D(t) = \frac{\bar{F}_{IL}(t)}{\frac{1}{2} \rho D L_{dyno} \bar{U}(t)^2} \quad (11)$$

The drag loads in the in-line direction that are reported in this section have not been adjusted to account for the inertial loads caused by the cylinder and testing apparatus which is itself accelerating in the continuously varying towing speed tests. Because the carriage accelerates or decelerates slowly these inertial loads are small. In the worst of cases these inertial loads are on the order of just 2% of the fluid drag loads and are much smaller than the typical variability observed in the recorded drag loads. If these tests had been conducted in a flume instead of towing tank, it is easy to show that provided that the  $\gamma$  parameter is kept at similar levels the Froude–Krylov forces due to the accelerating far field flow will similarly lead to inertial loads that are small compared to the fluid drag loads.

Investigating and presenting the stationary cylinder drags loads serves the following purposes: it is important to confirm that the *free-response* VIV tests which were conducted at Reynolds number above  $\sim 3.0 \times 10^5$ , were outside the ‘drag-crisis’ region and well into the supercritical Reynolds regime of the fixed cylinder. Additionally, the *fixed cylinder drag tests* serve as the basis against which the VIV amplified drag coefficients can be compared to.

### Results from the fixed cylinder drag tests

Fig. 16 shows the measured drag coefficient as a function of the Reynolds number for the *fixed cylinder drag tests*. The drag coefficient measured in the constant speed tests is shown in red or magenta colors whereas the ramp test results (*i.e.* variable towing speeds) are shown as continuous lines in blue and green color. The same color convention is used for Fig. 17 which shows the shedding frequency for the same tests. The shedding frequency shown in this plot is not an estimate but rather the actual vortex shedding frequency as computed from the instantaneous frequency of the measured oscillating drag forces in the cross-flow direction. Because the towing speed is not varied in a steady test, the results appear as vertical lines with the length of the vertical line representing the variability in the recorded drag loads while passing through the entire time-series with the moving window. Each red or magenta bar extends from the minimum to the maximum value of the moving average quantity observed over the full extent of the time series. In the time-varying flows of the ramp tests, the variability is demonstrated by the fact that repeated ramp tests do not measure the exact same drag loads. If ramp tests are repeated multiple times they can be used to characterize the drag coefficient variability that exists at high Reynolds numbers. The results measured in the ramp tests are in good agreement with the

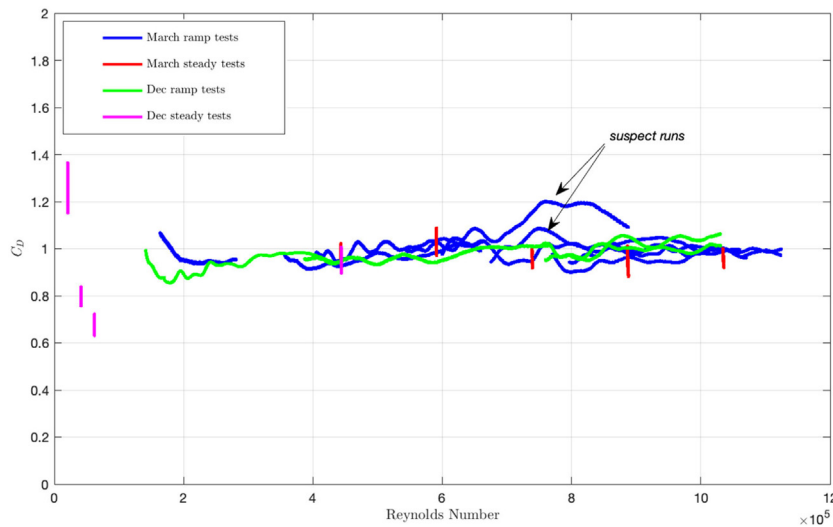


**Fig. 16.** Drag coefficient vs. Reynolds number from fixed cylinder tests.. (For interpretation of the references to color in this figure legend, the reader is referred to the web version of this article.)

constant speed results with the exception of a single ramp result between Reynolds numbers of  $7 \times 10^5$  to  $9 \times 10^5$  with the drag coefficient becoming as large as 1.2 which will be discussed in detail.

For the *fixed cylinder drag tests*, metal blanks were placed between the cylinders and supports to prevent the cylinder from moving and compressing the springs. For most of the tests and especially at Reynolds numbers below  $6 \times 10^5$ , these blanks were very effective with the recorded response amplitudes being smaller than  $\pm 0.1$  mm. For some of the very high Reynolds numbers cases the recorded response amplitudes might intermittently reach  $\pm 1$  mm. Careful examination of the cylinder responses and forces revealed that for the problematic case with a  $C_D \sim 1.2$ , the recorded cylinder motions were several times larger than what had been observed in the other test runs with response amplitudes approaching  $\pm 5$  mm. This was most likely the result of exciting a resonance for the entire cylinder and supporting test-rig. This suspicion is further confirmed by the results in Fig. 17 where the shedding frequency for this run has locked into a frequency of 1.45–1.5 Hz and the system continues to shed vortices at these frequencies even though the towing speed has increased showing a dramatic departure from the expected Strouhal relationship. This is consistent with lock-in of very high mass ratio cylinders and is typically seen in ‘in-air’ VIV tests where the mass ratios are usually on the order of  $10^2$  or  $10^3$ . While the test cylinder is fixed and prevented from moving with the use of the metal blanks, the actual system under consideration is not the spring-supported cylinder and linkages but rather the entire VIV testing apparatus and towing carriage and hence the effective mass ratio of the cylinder is not the low value of 1.56 but many times larger since the mass of the VIV testing apparatus and possibly a portion of the towing carriage/platform need to be included in the total mass calculation.

Note that the large variation observed in the shedding frequency at  $Re \sim 7.5 \times 10^5$  is an artifact of the instantaneous frequency calculation that occurred as the recorded cross-flow loads on either end of the cylinder went out-of-phase. As a result, the total cross-flow load which is the sum of the loads on either end of the cylinder went to zero and the instantaneous frequency also goes to zero. This only occurred for a small portion of the test-record and lasted 2–3 cycles whereas the instantaneous frequency for the remaining portion was between 1.5–1.6 Hz which is consistent with the expected Strouhal shedding frequency. The non-zero values shown are the result of computing and reporting the average of the instantaneous frequency using a moving-window that is approx. 5 cycles long and passes through the entire data record. It is unclear what caused this peculiar behavior in this steady speed test.

The maximum Reynolds number that was achieved in the fixed cylinder tests was considerably larger than the maximum Reynolds number possible in the *free-response* VIV tests. This is because the primary limitation was on the total drag load on the VIV test rig and the towing carriage. As will be demonstrated in the following section, the freely vibrating cylinder experiences drag loads nearly 2.5 times larger than the fixed cylinder drag loads which means that the testing rig’s maximum permissible drag load is reached at considerably lower towing velocities when the cylinder is in the spring-mounted arrangement and free to respond to the flow. With the exception of the two runs that showed abnormally high drag coefficients that were previously discussed, the fairly constant drag coefficients which are consistently in the range of 0.90 to 1.05 for  $Re > 2 \sim 3 \times 10^5$  are a very good indication that this is in fact the supercritical Reynolds regime.

Due to the limited time available for testing it was not possible to capture the entire drag-crisis region for this cylinder. The large variations recorded in the drag coefficients for the steady tests at  $Re \sim 2.1 \times 10^4$ ,  $Re \sim 3.1 \times 10^4$  and  $Re \sim 6.2 \times 10^4$ , with values ranging from  $\sim 1.3$  to  $\sim 0.65$ , indicates that this is the neighborhood of the drag crisis region for

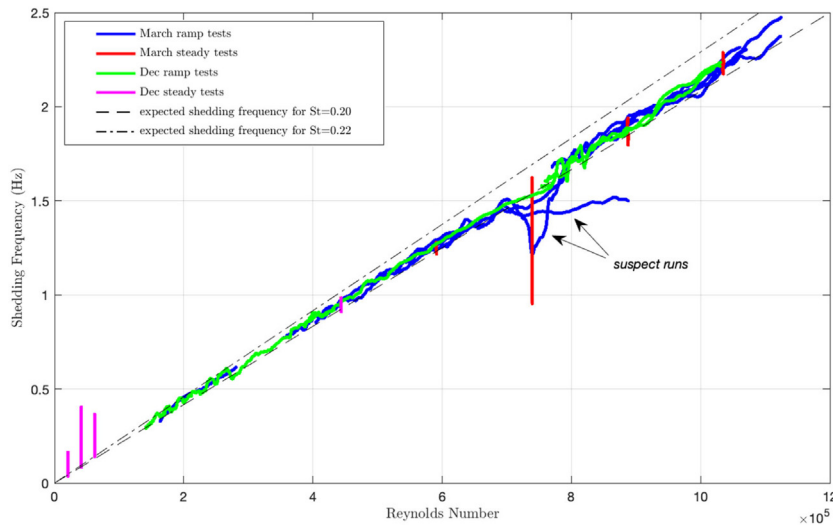


**Fig. 17.** Measured shedding frequency vs. Reynolds number from fixed cylinder tests.. (For interpretation of the references to color in this figure legend, the reader is referred to the web version of this article.)

the cylinder with the aspect ratio and surface roughness used in these experiments. Too few tests were conducted in this region to fully trace out the variability in the data and its full extent but the recorded data suggests that after a Reynolds number of approx.  $2 \times 10^5$  to  $3 \times 10^5$  the drag coefficient has recovered to a value of  $\sim 1.0$  and is in the supercritical Reynolds region. The ramp test recorded data showed some small amounts of variability with the drag coefficient values varying between 0.9 to 1.05–1.1 which is similar to the variability that was observed in the steady towing speed tests performed.

The fixed or stationary cylinder drag coefficients that were measured and shown here are in good agreement with the values reported by [Ding et al. \(2004\)](#) for their large roughness cylinder which had a similar surface roughness with the one used in this investigation. They show data that places the drag crisis approximately between  $Re \sim 9 \times 10^4$  and  $Re \sim 3 \times 10^5$  after which point the drag coefficient that they report has values of  $1.0 < C_D < 1.1$ . [Dahl et al. \(2010\)](#) show stationary cylinder drag coefficient values of  $0.85 < C_D < 0.9$  for the Reynolds range between  $3 \times 10^5 < Re < 4 \times 10^5$  and subsequently show that the drag coefficient recovers a value of  $C_D \sim 1.1$  by the time the Reynolds number exceeds  $\sim 5 \times 10^5$  which are in satisfactory agreement with the results shown here.

#### Drag coefficients measured during the free-response VIV tests

The large response amplitudes that are observed in *free-response* VIV tests are accompanied by significantly increased drag coefficients. It is illustrative to compare these VIV amplified drag coefficients to the usual values seen on fixed cylinders. [Fig. 18](#) shows the calculated drag coefficient from the *free-response* VIV tests that were conducted during the second round of testing in December of 2015. The contours cover the entire region where *self-excited* oscillations are possible and demonstrate the well-known effect of VIV amplified drag. The drag coefficient from fixed cylinder tests at the same Reynolds number is typically between 0.9 and 1.1 whereas for the freely vibrating cylinder drag coefficients values as large as 2.6 are observed. For reduced velocities greater than  $V_{Rn} > 5$ , the drag coefficient is nearly independent of the nominal reduced velocity value and has a nearly monotonic dependence on the response amplitude.

[Fig. 19](#) compares the measured drag coefficient values in these *free-response* VIV tests for reduced velocities between  $4.8 < V_{Rn} < 6.2$  with the modified drag amplification formula proposed by [Vandiver \(1983\)](#) nearly 40 years ago. Drag amplification estimates using both a stationary drag coefficient of 0.9 and 1.0 are shown since both of these values are representative of what was measured in the *fixed cylinder drag tests* and shown earlier in [Fig. 16](#). The reduced velocity has been intentionally been confined to range of  $4.8 < V_{Rn} < 6.2$  since this range typically corresponds to peak response conditions.

#### Appendix B. On the use of the true reduced velocity in free-response VIV data

In this investigation, the response amplitude and response frequency together with the lift and added mass coefficients are all intentionally presented as a function of the nominal reduced velocity,  $V_{Rn}$ , instead of the true reduced velocity,  $V_{Rvib}$ . For very low mass-ratio cylinders when the response data is plotted as a function of the true reduced velocity, a large amount of the response data collected ‘folds-under’ itself and occurs at the same value of true reduced velocity. This

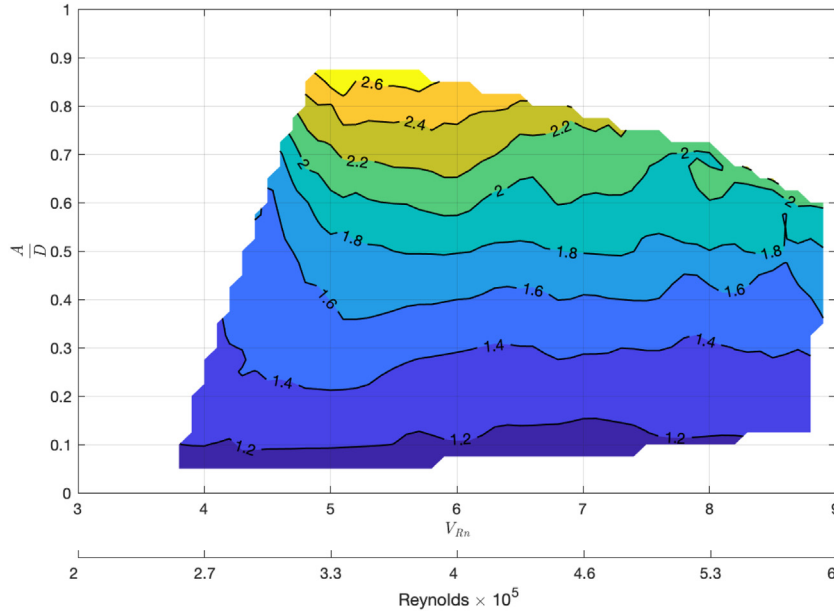


**Fig. 18.** Contours of VIV amplified drag coefficient ( $C_D$ ) for the December free-response VIV tests. (For interpretation of the references to color in this figure legend, the reader is referred to the web version of this article.)

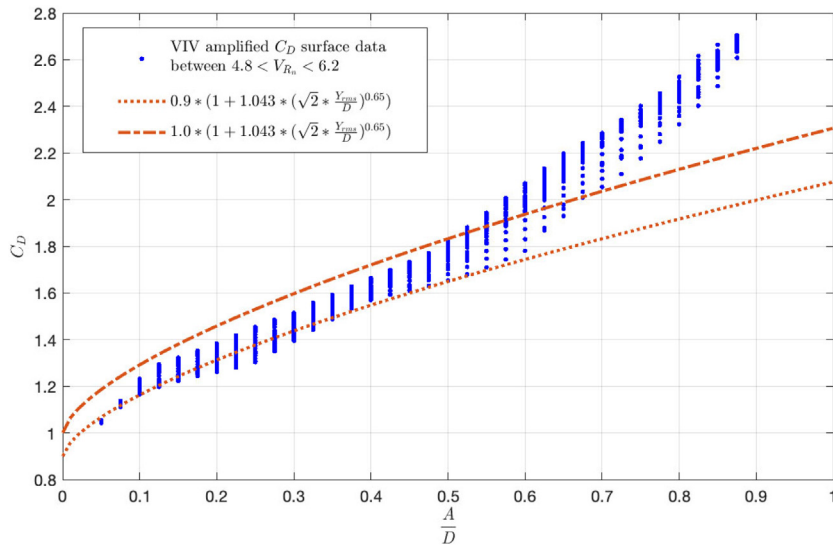


**Fig. 19.** Comparison of drag amplification formula with measured results in free-response VIV. (For interpretation of the references to color in this figure legend, the reader is referred to the web version of this article.)

happens because the fluid added mass has a large effect on the total system mass and the system's effective natural frequency. The implication is that most of the response information collected for nominal reduced velocities larger than the critical reduced velocity actually occurs at virtually the same value of true reduced velocity. This does not facilitate the comparisons between the ramp test and steady tests and makes it hard to account for differences in Reynolds number.

Fig. 20 shows the dimensionless response amplitude as a function of the true reduced velocity which itself is a function on the response frequency based on the definition in Eq. (9). The response data presented in this figure is identical to what was shown earlier in Fig. 7. Instead of showing each of the dependent variables (i.e. the response amplitude and the response frequency) against the independent variable (i.e. the nominal reduced velocity) the decision to plot quantities against the true-reduced velocity essentially results in a plot of one dependent variable against another. The response variability in the amplitude and frequency that was clearly evident in the steady towing speeds tests as vertical red lines now becomes much more complicated resembling Lissajous-like curves as a result of the small variations in both

response frequency and amplitude that occur simultaneously (*i.e.* there is a slight frequency and amplitude modulation in the *free-response* data even in steady flows). The vertical extent of the each red-curve still corresponds to the response amplitude variability (amplitude modulation) but now the horizontal width of the same curve represents the variation in response frequency (frequency modulation) and hence a slight variation in the true reduced velocity.

In this format, the comparison between steady test results and ramp test extracted results is more challenging but the same good agreement exists since the quantities being compared are identical to what was shown earlier in Fig. 7. The figure clearly demonstrates how the response data for all the high nominal reduced velocity values (*i.e.*  $V_{Rn} > \sim 5.5$ ) 'folds-under' itself with a large portion of the response curve 'folding-under' the peak response value. It is important to emphasize that this 'folding' of the high nominal reduced velocity data is not limited to the ramp test results but is also exhibited in the steady test results. For example, the results from the two steady tests at  $V_{Rn} \sim 6.5$  and  $V_{Rn} \sim 7.5$  fully overlap each other on this plot as a result of the response variability in the amplitude and the nearly identical (true) reduced velocity values that are a result of the decreasing added mass coefficients. These data points are now mapped to  $V_{Rvib}$  values of  $\sim 5.6$  and  $\sim 5.5$  and lie beneath the steady test result with the maximum amplitude that originally occurred at  $V_{Rn} \sim 5.5$  but has now been mapped to  $V_{Rvib} \sim 5.3$ . The steady test results originally corresponding to  $V_{Rn} \sim 7.5$  has now been drawn in another color to make it easier to distinguish the two constant speed tests. The figure includes a simplified schematic showing the differences between the cylinder's response path in accelerating and decelerating flows.

As discussed earlier, the towing velocity in these tests was never increased to sufficiently large values to enter the desynchronization region for this low mass-ratio cylinder. This becomes especially obvious in the  $A/D$  vs.  $V_{Rvib}$  plot which has no data extending past  $V_{Rvib} \sim 6$  for this spring-damping setting. The response data collected in this test is limited to the 'initial branch', the 'upper branch' and the transition to the beginning of the 'lower branch' of response. Despite the limitation of not being able to fully capture the desynchronization region, the lift coefficient surfaces shown earlier clearly included the peak lift coefficient value which was the necessary prerequisite to deduce whether Reynolds effects exist in the supercritical Reynolds regime. Another complication that arises due to the 'folding' of the response data is that there is no longer a direct conversion between the Reynolds number and the true reduced velocity. This makes it more challenging to present the *free-response* data in a manner that would easily illustrate any Reynolds effects which was a key objective in this investigation.

Fig. 21 shows the response amplitude measured in the second round of tests in December 2015 and illustrates the effect of increasing damping when the *free-response* results are plotted against the true reduced velocity. The neat curves of response amplitude vs. nominal reduced velocity which were shown in Fig. 12 now become much more complicated since the response amplitude is being plotted against the true reduced velocity which itself depends on the response frequency. When the *free-response* data is presented in this format, the figures show the variation of one dependent variable against another dependent variable. The increased damping causes the transition between the 'initial' and 'upper' branches to occur at larger values of true-reduced velocity. The curves gradually move from  $V_{Rvib} \sim 5.5$  to  $V_{Rvib} \sim 6$  and it appears that the 'upper' branch does not exist for damping values larger than  $\zeta > 0.23$  and possibly for  $\zeta > 0.20$ . The figure includes a simplified schematic demonstrating the data folding and the gradual shift towards larger values of true reduced velocity as the damping is increased.

When the lift and added mass coefficient surfaces are plotted against the true reduced velocity,  $V_{Rvib}$ , they are similarly affected by the issue of the response data 'folding under' itself. The primary reason one would try to show lift and added mass coefficient surfaces from *free-response* data against the true reduced velocity instead of the nominal reduced velocity is to allow the comparison with *forced-vibration* VIV test data. The data from *forced-vibration* tests is always shown in the literature as a function of the true reduced velocity because the cylinder's externally prescribed oscillation frequency is the only quantity available for non-dimensionalizing the flow speed in a *forced-vibration* test.

The issue of the low-mass ratio *free-response* data 'folding-under' itself becomes very important when presenting the coefficient information as a function of the true reduced velocity as shown in Fig. 22. The coefficient surfaces are no longer smooth and slowly varying surfaces. The lift coefficient and added mass coefficient data is identical to what was used to create the smooth surfaces of Fig. 13 but is now 'folded-over' in a complicated manner similar to response information discussed above. Attempting to fit surfaces when the results are plotted against the true reduced velocity leads to these complicated surfaces that show extensive localized variation with many local minima and maxima. The localized variation that appears in both coefficients surfaces is the result of attempting to fit a single coefficient surface to substantially different *free-response* data which has 'folded-under' itself and occurs at similar values of true reduced velocity. The 'folding' of the low mass-ratio response amplitude data when plotting the *free-response* test results as a function of the true reduced velocity instead of the nominal reduced velocity, occurs because the fluid added mass has a large effect on the total system mass and the system's effective natural frequency. The problem is exacerbated at low-mass ratios like the one corresponding to the cylinder used in this investigation.

The problems associated with the overlapping *free-response* data when presenting coefficients in terms of the true reduced velocity is best demonstrated through a series of examples. Fig. 23 demonstrates the lift and added mass coefficient surfaces that can be created if the *free-response* data is limited to specific regions of nominal-reduced velocity before the surface fitting is attempted in the  $A/D$  vs.  $V_{Rvib}$  domain. This is done in an attempt to avoid combining and averaging dissimilar response data and would ideally be based on grouping the *free-response* data collected based on the exact vortex shedding patterns in the wake in a manner similar to what Morse and Williamson (2009a,b) did for their forced-vibration data. Zhao et al. (2014) were able to identify and to characterize the competition between the '2S'-'2P<sub>0</sub>'



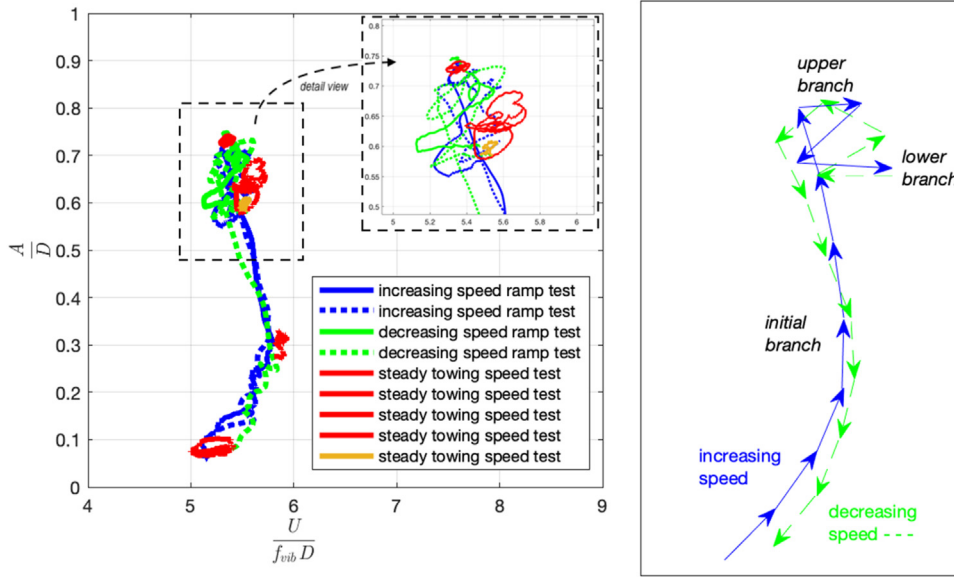


**Fig. 20.** Dimensionless response amplitude vs. true reduced velocity for March tests with stiff springs ( $F_n \sim 0.90$  Hz) and  $\zeta = 0.09$ . Compare with Fig. 7. (For interpretation of the references to color in this figure legend, the reader is referred to the web version of this article.)

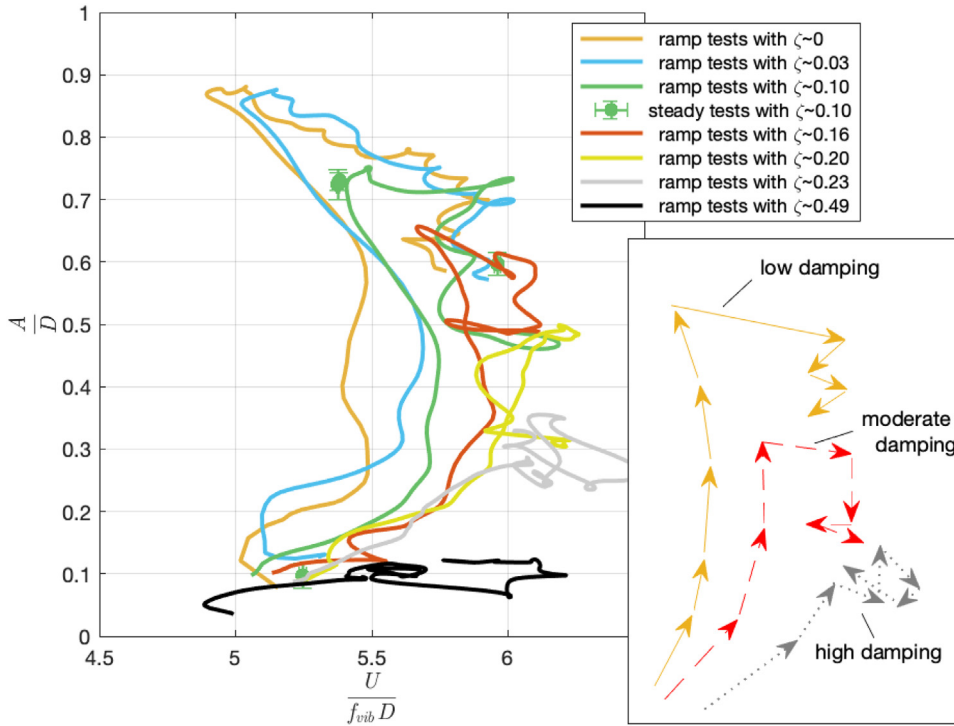


**Fig. 21.** Response amplitude vs. true reduced velocity ( $V_{Rvib}$ ) for December tests with soft springs ( $F_n \sim 0.69$  Hz) and 7 different damping levels. Compare with Fig. 12. (For interpretation of the references to color in this figure legend, the reader is referred to the web version of this article.)

and the '2P<sub>o</sub>'-'2P' regions. They found the exact percentage of time that their freely vibrating cylinder spent in each of the '2S', '2P' and '2P<sub>o</sub>' modes for each value of nominal reduced velocity tested. Because their tests were at much lower Reynolds numbers and had a larger mass ratio it is not known if the same nominal reduced velocity ranges would apply for the cylinder and Reynolds numbers used in this investigation. Furthermore, because their experimental setup had very small amounts of damping and thus responded with large response amplitudes, it is not known how their identified

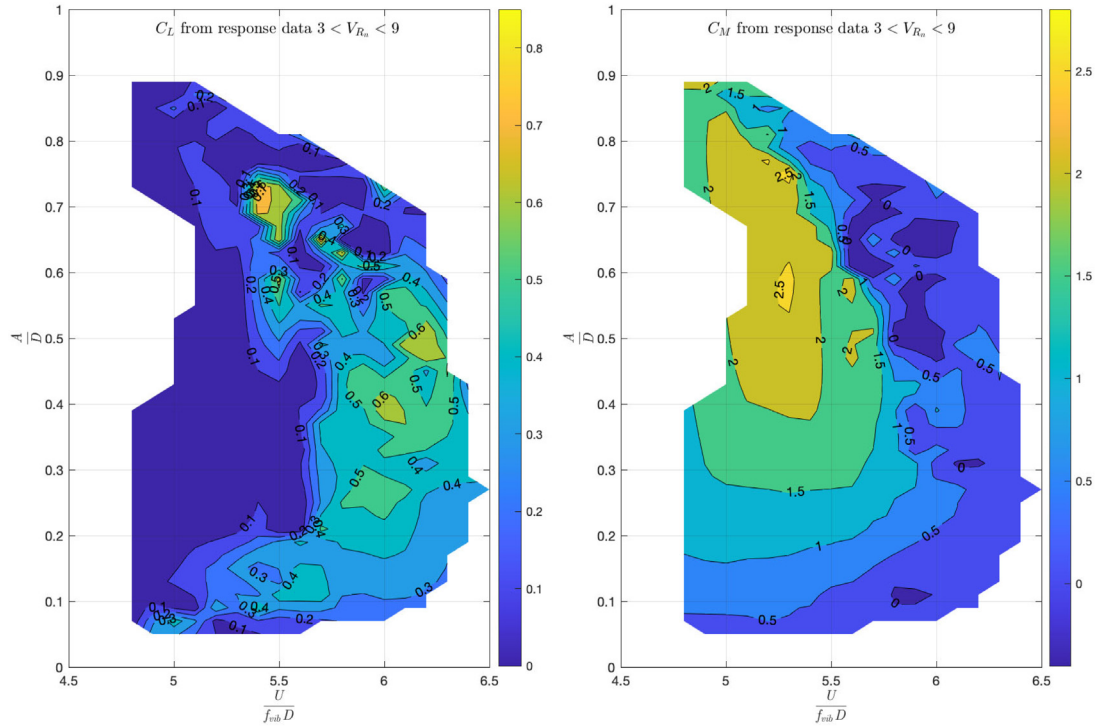


**Fig. 22.**  $C_L$  contours (LEFT) and  $C_M$  contours (RIGHT) for December tests with Soft Springs with  $F_n \sim 0.69$  Hz. Coefficients computed using all available response data ( $3 < V_{Rn} < 9$  collected in the *free-response* tests. (For interpretation of the references to color in this figure legend, the reader is referred to the web version of this article.)

$V_{Rn}$  ranges would change for higher amounts of damping (*i.e.* at smaller response amplitudes). Because detailed wake visualizations were not available in this investigation, the data was grouped in a very approximate manner based on the expected ranges of the ‘initial-branch’, the ‘upper-branch’ and the ‘lower-branch’ in the nominal reduced velocity domain. The response data corresponding to  $3 < V_{Rn} < 6$ , will include the response data from the initial branch and at least the beginning of the upper branch data. The subsequent ranges of  $6 < V_{Rn} < 7$ ,  $7 < V_{Rn} < 8$ ,  $8 < V_{Rn} < 9$ , correspond to the transitions from the ‘upper-branches’ to the ‘lower-branches’ at larger nominal reduced velocity values, all of which overlap in the  $V_{Rvib}$  domain and are associated with the large decrease in the added mass coefficient that occur.

Inspecting these individual coefficient surfaces reveals that depending on which part of the original  $V_{Rn}$  response domain was used to create the surfaces, the coefficients can take on significantly different values when plotted against the true reduced velocity. This happens because apart from the expected variation of the lift and added mass coefficients with amplitude and true reduced velocity, the coefficient values in certain regions of the amplitude vs. true reduced velocity plane can also depend on the wake state. This was clearly shown in the observations Morse and Williamson (2009a,b) which showed that the ‘2P<sub>0</sub>’ region fully overlaps the ‘2S’ and ‘2P’ regions and the coefficient values can show significant difference depending on the type of wake structure at the same value of true reduced velocity. The nominal reduced velocity ranges for the individual sub-plots shown here were chosen in a very approximate way to attempt and group the free-response data based on their expected or believed wake patterns. Note that, each of the individual coefficient surfaces shown in Fig. 23 varies smoothly. The coefficient surfaces shown previously in Fig. 22, which showed considerable localized variation, are effectively the result of stacking each of the four individual coefficient surfaces shown in Fig. 23 on top of each other and averaging the results.

It is clear that in certain regions of the  $A/D$  vs.  $V_{Rvib}$  domain the coefficients can take on very different values depending on the response data used. The process of fitting a single surface that averages very different coefficient values occurring at the same true reduced velocity, results in considerable localized variation shown in the in Fig. 22. For example, the added mass coefficient that corresponds to the response in the initial branch is very different from the near zero added mass coefficients in the lower branch and averaging these quantities in a single coefficient surface is a gross over-simplification. The same exercise could be repeated in a more rigorous manner if wake visualizations were available to inform and guide the selection and grouping of the *free-response* VIV data into specific nominal reduced velocity ranges.

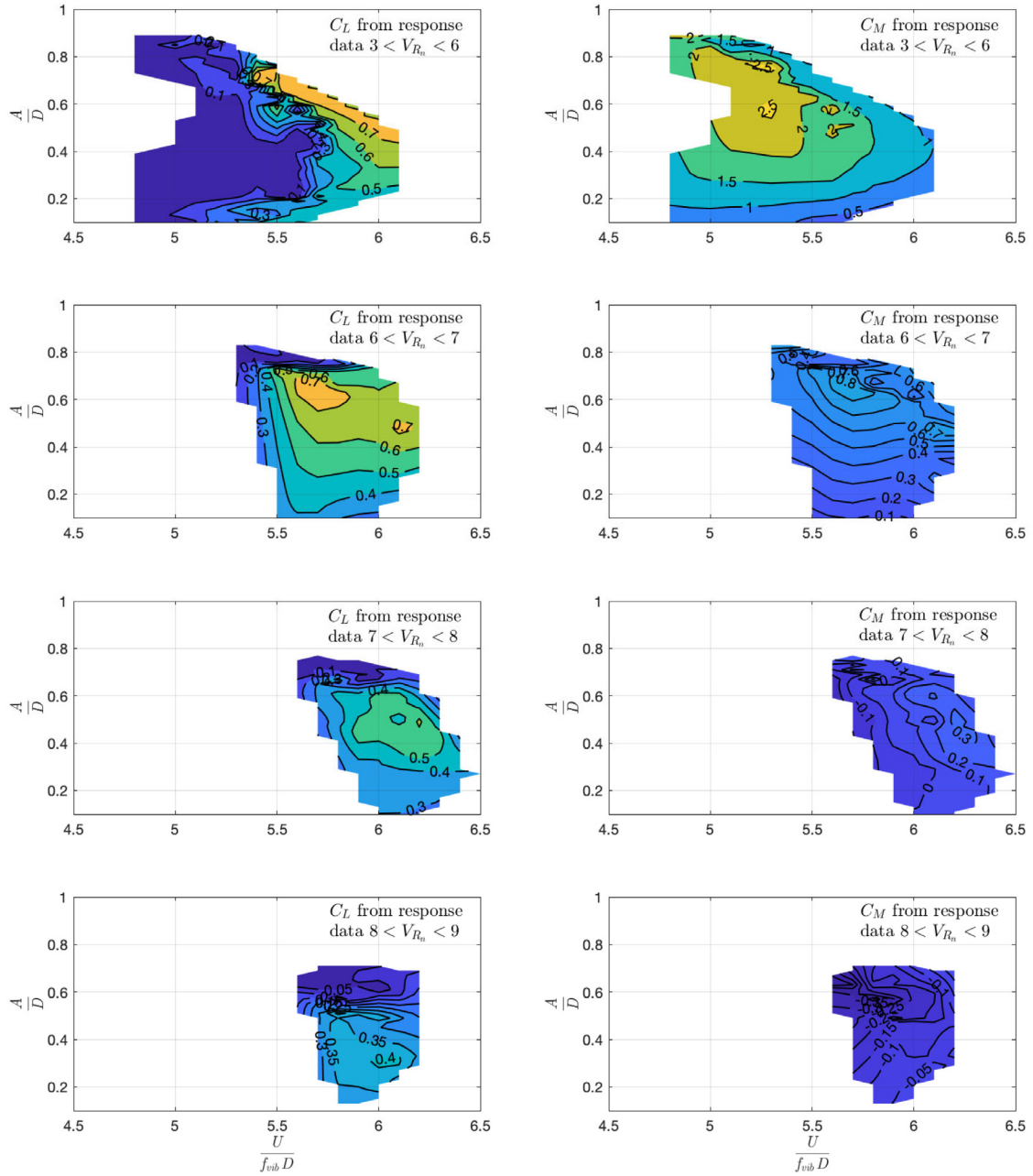


**Fig. 23.**  $C_L$  contours (LEFT) and  $C_M$  contours (RIGHT) for Dec. tests with Soft Springs with  $F_n \sim 0.69$  Hz. Coefficients computed using specific ranges of response data recorded in the tests. Refer to individual figure annotations for details on the specified range of response data (i.e.  $V_{Rn}$  values) used in each case. (For interpretation of the references to color in this figure legend, the reader is referred to the web version of this article.)

To summarize, when plotting the *free-response* VIV data of low mass-ratio cylinders against the true reduced velocity instead of the nominal reduced velocity, a large portion the data from 'the upper' and the beginning of the 'lower branches' is observed to occur at very similar values of true reduced velocity and the response curve looks like they have 'folded under' themselves. This is a result of the rapidly decreasing added mass coefficient in this region and the problem is exacerbated due to the low-mass ratio of the cylinder which means that the fluid added mass contributes significantly to the total oscillatory inertia. This greatly complicates the proper presentation of the coefficient data as function of the true reduced velocity and one needs to exercise caution when interpreting these results as the coefficients corresponding to different wake regions may have been averaged in an overly simplistic manner.

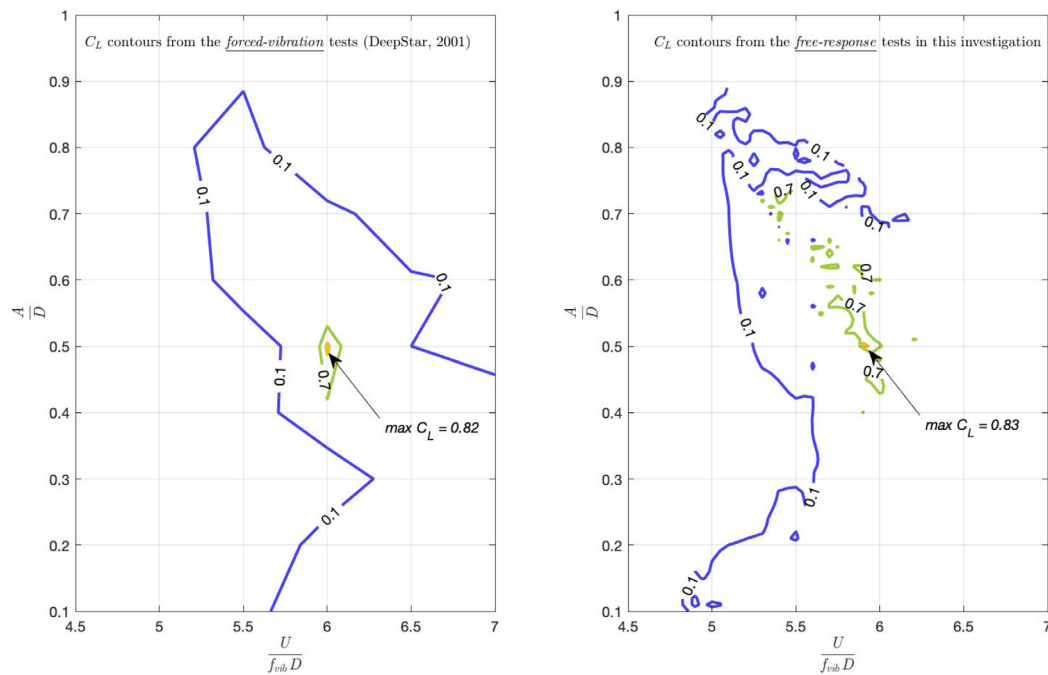


**Fig. 24.**  $C_L$  contours from the DeepStar forced-vibration tests (LEFT) and those computed after compiling all the available free-response data in this investigation (RIGHT). (For interpretation of the references to color in this figure legend, the reader is referred to the web version of this article.)

#### Comparison of results from free-response VIV tests with the forced-vibration measurements

The main reason for showing the *free-response* coefficient information as a function of the true-reduced velocity, despite the issues discussed earlier, is to facilitate the comparison with the available *forced-vibration* data at similar supercritical Reynolds numbers. Since this investigation found that the supercritical Reynolds number effects were weak, the lift coefficient information computed from both supercritical Reynolds ranges can be combined into a single set of coefficients. Only results from the increasing speed March ramp tests were used and these were further complemented by the more complete coefficient surfaces computed in the December tests. The key elements of the resulting coefficients after combining all these *free-response* data are shown in Fig. 24.

In the DeepStar *forced-vibration* tests that were conducted in 2001–2003 at the same facility (DeepStar, 2003), the controlled oscillation amplitude was varied from 0.1 to 0.9D in steps of 0.2 diameters and both the towing speed and forcing frequency were varied in a manner that resulted in the true reduced velocity ranging from 3 to 9 in increments of 0.5. In the tests with the smaller prescribed oscillation amplitudes the Reynolds number varied between  $\sim 4 \times 10^5 < Re < \sim 7 \times 10^5$ , whereas in the tests with the larger prescribed amplitudes of 0.9D the Reynolds number range was kept lower at  $\sim 2 \times 10^5 < Re < \sim 4 \times 10^5$  to limit the total drag loads on the VIV testing apparatus and the towing carriage.

The comparison between the lift coefficients measured in the *forced-vibration* DeepStar tests and those computed in this investigation using *free-response* tests will be limited to the key features observed such as the maximum lift coefficient and the approximate location of the limit cycle amplitude which are shown in Fig. 24. The maximum lift coefficient measured during the DeepStar *forced-vibration* experiments was 0.82 and occurred at  $A/D = 0.5$  &  $V_{Rvib} = 6$  which compares nicely with the maximum  $C_L$  value of 0.83 occurring  $A/D = 0.5$  &  $V_{Rvib} = 5.9$  obtained from the *free-response* tests in this investigation. Because the *free-response* tests do not result in negative lift coefficients, the  $C_L = 0$  contour is not well captured in the contour surfaces. The  $C_L = 0.1$  contours are being used here to approximate the limit cycle amplitude (*i.e.*  $C_L = 0$ ) and these also compare nicely between the *forced* and *free-response* data, with the later systematically occurring at slightly lower true reduced velocity values. Because the towing velocity in these *free-response* tests was never increased to large enough values to result in full desynchronization, the  $C_L = 0.1$  contours do not extend beyond  $V_{Rvib} > 6$ .

In addition to the approximated limit-cycle contours and the maxima, the general shapes of the lift coefficient surfaces are similar but the surfaces created using the *free-response* data in this investigation shows extensive localized variation corresponding to local minima or local maxima that cannot be compared directly to the coefficient surface from the *forced-vibration* tests because that test matrix was not refined enough to show these finer details. The *forced-vibration* test matrix that was used in that investigation spaced the testing grid points at  $A/D$  steps of 0.2 and true reduced velocity steps of 0.5, which is not refined enough for comparison to the continuous  $V_{Rvib}$  and  $A/D$  variation that exists in the *free-response* tests of this investigation. The overall agreement between the main features in the *forced-vibration* and *free-response* lift

coefficient is good considering the many subtle differences that can exist between *forced-vibration* and *free-response* model testing but cannot be covered in detail here.

Long risers or cables exposed to real ocean conditions typically respond at high mode numbers. At these high mode numbers, a flexible cylinder or cable will choose to respond at a mode number such that it is always in the reduced velocity region that leads to peak response. The peak lift coefficient and its immediate neighborhood was well captured in these tests as demonstrated earlier. The lift and added mass coefficients computed in this investigation are more than adequate for our intended purpose of incorporating them into a semi-empirical VIV prediction program like SHEAR7 that employs a strip-theory approach for predicting the VIV response of long slender risers or cables.

## References

- Bishop, R.E.D., Hassan, A.Y., 1964. The lift and drag forces on a circular cylinder oscillating in a flowing fluid. *Proc. R. Soc. A* 5, 1–75.
- Blevins, R.D., 1990. *Flow-Induced Vibrations*. Van Nostrand Reinhold, New York, NY.
- Blevins, R.D., 2009. Models for vortex-induced vibration of cylinders based on measured forces. *J. Fluids Eng.* 131 (10).
- Blevins, R.D., Coughran, C.S., 2009. Experimental investigation of vortex-induced vibration in one and two dimensions with variable mass, damping, and Reynolds number. *J. Fluids Eng.* 131 (10).
- Constantinides, Y., Raghavan, K., Karayaka, M., Spencer, D., 2013. Tandem Riser Hydrodynamic Tests at Prototype Reynolds Number. In: ASME 2013 32nd International Conference on Offshore Mechanics and Arctic Engineering, June 9th –14th, 2013, Nantes, France, OMAE2013-10951.
- Dahl, J.M., Hover, F.S., Triantafyllou, M.S., 2006. Two-degree-of-freedom vortex-induced vibrations using a force assisted apparatus. *J. Fluids Struct.* 22 (6–7), 807–818.
- Dahl, J.M., Hover, F.S., Triantafyllou, M.S., Oakley, O.H., 2010. Dual resonance in vortex-induced vibration at subcritical and supercritical Reynolds numbers. *J. Fluid Mech.* 643, 395–424.
- DeepStar, 2003. High Reynolds number experiment dataset, vortex induced vibration data repository. website accessed 2020, <http://web.mit.edu/towtank/www/vivdr/index.html>.
- Ding, Z.J., Balasubramanian, S., Lokken, R.T., Yung, T.-W., 2004. Lift and damping characteristics of bare and straked cylinder at riser scale Reynolds numbers. In: Offshore Technology Conference, Offshore Technology Conference, May 3rd –6th, Houston, Texas, OTC 16341.
- Gopalkrishnan, R., 1993. *Vortex-Induced Forces on Oscillating Bluff Cylinders* (Ph. D. Thesis). Massachusetts Institute of Technology, Cambridge, MA, USA.
- Govardhan, R.N., Williamson, C.H.K., 2000. Modes of vortex formation and frequency response of a freely vibrating cylinder. *J. Fluid Mech.* 420, 85–130.
- Govardhan, R.N., Williamson, C.H.K., 2006. Defining the 'Modified Griffin Plot' in vortex-induced vibration: Revealing the effects of Reynolds number using controlled damping. *J. Fluid Mech.* 561, 147–180.
- Klamo, J.T., Leonard, A., Roshko, A., 2005. On the maximum amplitude for a freely vibrating cylinder in cross-flow. *J. Fluids Struct.* 21, 429–434.
- Lee, J.H., Bernitsas, M.M., 2011. High-damping, high-Reynolds VIV tests for energy harvesting using the VIVACE converter. *Ocean Eng.* 38 (16), 1697–1712.
- Leonard, A., Roshko, A., 2001. Aspects of flow-induced vibration. *J. Fluids Struct.* 15, 415–425.
- Lie, H., Braaten, H., Szewalek, J., Russo, M., Baarholm, R., 2013. Drilling Riser VIV Tests with Prototype Reynolds Numbers. In: ASME 2013 32nd International Conference on Offshore Mechanics and Arctic Engineering, June 9th –14th, 2013, Nantes, France, OMAE2013-11643.
- Morse, T.L., Williamson, C.H.K., 2009a. Fluid forcing, wake modes, and transitions for a cylinder undergoing controlled oscillations. *J. Fluid Struct.* 25, 697–712.
- Morse, T.L., Williamson, C.H.K., 2009b. Prediction of vortex-induced vibration response by employing controlled motion. *J. Fluid Mech.* 634, 5–39.
- Morse, T.L., Williamson, C.H.K., 2010. Steady, unsteady and transient vortex-induced vibration predicted using controlled motion data. *J. Fluid Mech.* 649, 429–451.
- Paidoussis, M., 2003. *Fluid-Structure Interactions, Volume 2*. Academic Press.
- Raghavan, K., Bernitsas, M.M., 2010. Experimental investigation of Reynolds number effect on vortex induced vibration of rigid circular cylinder on elastic supports. *Ocean Eng.* 38–5, 719–731.
- Resvanis, T.L., 2014. *Vortex-Induced Vibration of Flexible Cylinders in Time-Varying Flows* (Ph.D. Thesis). Massachusetts Institute of Technology, Cambridge, MA, USA.
- Resvanis, T.L., Jhingran, V., Vandiver, J.K., Liapis, S., 2012. Reynolds number effects on the vortex-induced vibration of flexible marine risers. In: ASME 2012 31st International Conference on Offshore Mechanics and Arctic Engineering, July 1st – 6th, 2012, Rio De Janeiro, Brazil, OMAE2012-83565.
- Resvanis, T.L., Vandiver, J.K., 2017. Response variability in flexible cylinder VIV model test data. In: ASME 2017 36th International Conference on Ocean, Offshore and Arctic Engineering, June 25th – 30th, Trondheim, Norway, OMAE2017-61516.
- Resvanis, T.L., Vandiver, J.K., Fu, S., 2015. Ramp Tests: A Novel Approach to VIV Model Testing of Flexible Cylinders Using Continuously Varying Towing Speeds. In: ASME 2015 34th International Conference on Ocean, Offshore and Arctic Engineering, May 31st – June 5th, St. John's, NL, Canada, OMAE2015-42286.
- Sarpkaya, T., 2004. A critical review of the intrinsic nature of vortex-induced vibrations. *J. Fluids Struct.* 19–4, 389–447.
- Spencer, D., 2004. High Reynolds Number Cylinder Vortex Induced Vibration Test Apparatus. Oceanic Consulting Co. INT062-1, St. John's, Newfoundland, Canada.
- Sumer, B.M., Fredsoe, J., 2006. *Hydrodynamics Around Cylindrical Structures (Advanced Series on Ocean Engineering – Volume 26)*. World Scientific Publishing Co. Pte. Ltd, Singapore.
- Swithenbank, S.B., Vandiver, J.K., Larsen, C.M., Lie, H., 2008. Reynolds number dependence of flexible cylinder VIV response data. In: ASME 2008 27th International Conference on Ocean, Offshore and Arctic Engineering, June 15th – 20th, Estoril, Portugal, OMAE2008-57045.
- Vandiver, J.K., 1983. Drag Coefficients of Long Flexible Cylinders. In: Offshore Technology Conference, May 2nd – 5th, Houston, Texas, OTC 4490.
- Vandiver, J.K., 2012. Damping parameters for flow induced vibration. *J. Fluids Struct.* 35, 105–119.
- Vandiver, J.K., Resvanis, T.L., 2015. Improving the State of the Art of High Reynolds Number VIV Model Testing of Ocean Risers. Technical Report, Massachusetts Institute of Technology.
- Venugopal, M., 1996. *Damping and Response of a Flexible Cylinder in a Current* (Ph.D. thesis). Massachusetts Institute of Technology, Cambridge, MA.
- Williamson, C.H.K., Govardhan, R.N., 2004. Vortex-induced vibrations. *Annu. Rev. Fluid Mech.* 3, 413–455.
- Williamson, C.H.K., Roshko, A., 1988. Vortex formation in the wake of an oscillating cylinder. *J. Fluids Struct.* 2, 355–381.



- Yin, D., Lie, H., Baarholm, R.J., 2017, Prototype Reynolds Number VIV Tests on a Full-Scale Rigid Riser. In: ASME 2017 36th International Conference on Ocean, Offshore and Arctic Engineering, June 25th – 30th, Trondheim, Norway, OMAE2017-61415.
- Yin, D., Lie, H., Baarholm, R., 2018. Prototype Reynolds number vortex-induced vibration tests on a full-scale rigid riser. *J. Offshore Mech. Arct. Eng.* 140.
- Yin, D., Lie, H., Wu, J., 2020. Structural and hydrodynamic aspects of steel lazy wave riser in deepwater. *J. Offshore Mech. Arct. Eng.* (142).
- Zhao, J., Leontini, J.S., Lo Jacono, D., Sheridan, J., 2014. Chaotic vortex induced vibrations. *Phys. Fluids* (26).